2022

Advanced techniques for analyzing time-frequency dynamics of BOLD activity in schizophrenia

BOSTON UNIVERSITY

SCHOOL OF MEDICINE

Thesis

ADVANCED TECHNIQUES FOR ANALYZING TIME-FREQUENCY DYNAMICS OF BOLD ACTIVITY IN SCHIZOPHRENIA

by

SAMUEL PETER BUCK

B.S., Purdue University, 2019

Submitted in partial fulfillment of the

requirements for the degree of

Master of Science

2022

Approved by

First Reader

Kevin C Thomas, Ph.D.
Professor of Anatomy and Neurobiology

Second Reader

Itamar Ronen, Ph.D.
Professor of Radiology
Leiden University Medical Center

Third Reader

Xiaopeng Song, Ph.D.
Research Fellow in Psychiatry
McLean Hospital
Harvard Medical School

ACKNOWLEDGEMENTS

I'd like to begin by thanking my readers, each of whom contributed uniquely to this project's success. Dr. Thomas, for his encouragement of my interests in psychiatric imaging, his patience with my eccentricities, and his constant belief in my potential. Dr. Ronen, for his encouragement of my often esoteric technical questions and for introducing me to faculty at McLean hospital, with whom he correctively believed I'd fit. Dr. Song, for his suggestion of the Hilbert-Huang transform and his encouragement and guidance as I learned to work with fMRI time-series data. I couldn't have asked for a more generous or experienced group of readers. Additionally, my thanks to Dr. Fei Du and Dr. Dost Öngür at McLean Hospital for the opportunity to work with their group, and for their helpful feedback at various stages of the project. It has, and will continue to be, an honor and pleasure to work with everybody at McLean.

My endless thanks to my friends who aided me, both with their careful feedback and, more importantly, their companionship. Tim Stump, Hannah Sugarman, and of course my perpetual proofreader Rachel Brown: this would be entirely unreadable without your help. Additionally, I would be remiss if I did not thank Dr. Janusz Konrad, of the Boston University College of Engineering, for the LaTeX template used as the basis for typesetting this document.

Finally, I must extend my everlasting gratitude to Dr. Dan Foti and Keisha Novak from Purdue University for sparking my interest in both psychosis research and time-frequency analysis. Without the supportive environment they fostered, I would never have built the wide collection of skills which were vital for this project.

ADVANCED TECHNIQUES FOR ANALYZING TIME-FREQUENCY DYNAMICS OF BOLD ACTIVITY IN SCHIZOPHRENIA

SAMUEL PETER BUCK

ABSTRACT

Magnetic resonance imaging of neuronal activity is one of the most promising techniques in modern psychiatric research. While clear functional links with phenotypic variables have been established and detailed networks of activity robustly identified, fMRI scans have not yet yielded the robust biomarkers of psychiatric diseases, such as schizophrenia, which would allow for their use as a clinical diagnostic tool. One possible explanation for the lack of such results is that neural activity is highly nonstationary, whereas most analysis techniques assume that signal properties remain relatively static over time. Time-frequency analysis is a family of analytic techniques which do not assume that data is stationary, and thus is well suited to the analysis of neural time series. Resting state fMRI scans from a publicly available dataset were decomposed using the Wavelet transform and Hilbert Huang Transform, techniques from time-frequency analysis. The results of these processes were then used as the basis for calculating several properties of the fMRI signal within each voxel. The wavelet transform, a simpler technique, generated measures which showed broad differences between patients with schizophrenia and healthy controls but failed to reach statistical significance in the vast majority of situations. The Hilbert Huang transform, in contrast, showed significant increases in certain measures throughout areas associated with sensory processing, dysfunction in which is a symptom of schizophrenia. These results support the use of analysis techniques able to capture the nonstationarities in neural data and encourages the use of such techniques to explore the nature of the neural differences in psychiatric disorders.

TABLE OF CONTENTS

LIST OF FIGURES

LIST OF ABBREVIATIONS

ALFF	.....	Amplitude of Low Frequency Fluctuations
BOLD	.....	Blood Oxygenation Level Dependent
COBRE	.....	Center of Biomedical Research Excellence
dALFF	.....	Dynamic Amplitude of Low Frequency Fluctuations
DFT	.....	Discrete Fourier Transform
DMN	.....	Default Mode Network
DSM	.....	Diagnostic and Statistical Manual (of Mental Disorders)
EEG	.....	Electroencephalography
EMD	.....	Empirical Mode Decomposition
fMRI	.....	Functional Magnetic Resonance Imaging
FPN	.....	Frontoparietal (Control) Network
HHT	.....	Hilbert Huang Transform
HWF	.....	Hilbert Weighted Frequency
ICA	.....	Independent Component Analysis
IMF	.....	Intrinsic Mode Function
KCC	.....	Kendall's Coefficient of Concordance
MIP	.....	Maximum Intensity Projection
MNI	.....	Montreal Neurological Institute
MPRAGE	.....	Magnetization Prepared Rapid Acquisition Gradient Echo
MRI	.....	Magnetic Resonance Imaging
PFC	.....	Prefrontal Cortex

QOL	.....	Quality of Life
ROI	.....	Region of Interest
RS-fMRI	.....	Resting State Functional Magnetic Resonance Imaging
SCID	.....	Structured Clinical Interview for DSM Disorders
SPM	.....	Statistical Parametric Mapping
STFT	.....	Short Time Fourier Transform
WT	.....	Wavelet Transform

INTRODUCTION

Schizophrenia represents one of the most promising research targets for modern neuroscience. The disease is the most prominent member of the class of psychiatric conditions known as psychotic disorders, which are broadly characterized by deficits in reality testing – a patient's ability to identify and interact with the world around them (Arciniegas, 2015; Kelleher and Cannon, 2016; Parnas et al., 2010). Because this impact is so dramatic, understanding and treating psychosis has long been a goal of psychiatric investigations.

In the United States, roughly 100,000 people are diagnosed with a psychotic disorder per annum, with a lifetime prevalence rate for schizophrenia for the entire population between 0.4% and 0.7% (Simon et al., 2017; Wu et al., 2005; Saha et al., 2005; Simeone et al., 2015). Patients consistently report a significantly decreased quality of life (QOL) compared to healthy controls, a finding which tracks multiple measures of symptom and functional severity (Dong et al., 2019; Vrbova et al., 2017). Family members and caregivers also report a significant negative impact to their QOL (Yerriah et al., 2021; Hsiao et al., 2020). On a societal level, patients pose an economic burden: those diagnosed with schizophrenia are less likely to be employed and have far lower cumulative lifetime earnings than healthy controls (Hakulinen et al., 2019). Globally, societal cost per patient varies by nationality and social environment, but is estimated to be many thousands of dollars per year (Jin and Mosweu, 2017).

Psychotic disorders are highly heterogeneous. While psychosis is defined as deficits in reality testing, the criteria included in the Diagnostic and Statistical Manual of Mental Disorders (DSM) for schizophrenia specifies five key features, two or more of which suggest a diagnosis of schizophrenia (American Psychiatric Association, 2013, pp. 87-99). Delusions (fixed beliefs which do not effectively respond to contradictory evidence) and hallucinations (perceptual experiences which do not reflect sensory

stimulus) are often collectively described as positive symptoms (Stepnicki et al., 2018). Disorganized speech and disorganized or catatonic behavior, which can present as difficulties in properly forming sentences or engaging in goal-directed activities, are referred to as disorganized symptoms (Kwapil et al., 2018). The fifth feature, negative symptoms, presents as a lack of motivation (*avolition*) or a diminished ability to experience pleasure (*anhedonia*).

The significant harms caused by schizophrenia and the distinctiveness of its symptoms have made it a promising target of research for over a century (Andreasen and Carpenter, 1993). Because symptoms impact goal-directed behavior, schizophrenia is thought to reflect dysfunction surrounding the neurotransmitter dopamine, which is implicated in reward processing (Arias-Carrión et al., 2010). Dopamine's role is further highlighted by the chemical properties of psychopharmacological treatments for psychosis, which often involve binding affinity for dopaminergic neurons (Boyd and Mailman, 2012; Savica and Benarroch, 2014; Jauhar et al., 2017). In addition to dopamine, there is converging evidence of a significant role for the neurotransmitter glutamate, which has been linked to deficits in working memory and to aberrant connections in the frontoparietal network (Schmidt et al., 2015). On a systems scale, disrupted interactions between the prefrontal and perceptual cortices prompted Friston and Frith to describe schizophrenia as a "disconnection syndrome" (Friston and Frith, 1995). Under this understanding, different areas of the brain experience abnormal levels of functional segregation, failing to interact at contextually appropriate times, a model which has been bolstered by evidence from modern functional neuroimaging (Friston et al., 2016).

In order to investigate models of neural function and dysfunction, psychiatric neuroscientists measure a variety of different physiological quantities. Electroencephalography (EEG), for example, measures the electrical potential on the surface of the head,

providing evidence on the time course of neural activity within the brain. The high temporal resolution of this technique can shed light on the differences between different stages of cognition, and have been used to explore the impact of psychosis on the stages of reward processing (Novak and Foti, 2015; Clayson et al., 2019). Because many theories involving psychosis involve predictions about the activity of different areas of the brain, however, functional magnetic resonance imaging (fMRI) has also become a state of the art tool for psychosis research (Menon and Crottaz-Herbette, 2005). fMRI, which reflects neuronal metabolism throughout the three dimensional volume of the brain, can reveal which areas become more active when a person engages certain cognitive processes (Ogawa et al., 1990; Friston et al., 1996). In clinical research, examining the areas which show different activity in patients and healthy controls can reveal spatial loci for dysfunctional processes (Gluck et al., 2016).

Studies using fMRI have explored the way task-related activation differs between patients with schizophrenia and those without any diagnosis. Given the cognitive symptoms observed in schizophrenia, it is not surprising that many of these findings involve the prefrontal cortex (PFC), the area of the brain most responsible for higher cognition (Gluck et al., 2016). Tasks which measure executive function are often found to preferentially activate the dorsolateral PFC, activations which are impaired in psychosis patients (Orellana and Slachevsky, 2013). In general, the specific functional loci which appear to activate differently in schizophrenia are diffuse and inconsistent in the literature (Gur and Gur, 2010).

Instead of identifying areas which activate more or less strongly in schizophrenia, more compelling results come from measuring the connections between different brain areas. Connections between networks are inferred by measuring the signal within a single voxel over time, and identifying which voxels are behaving similarly (Biswal et al., 1995; Friston, 2011). By identifying collections of voxels with similar patterns

of activation, Yeo et al. defined a series of functional networks which have been thoroughly investigated in subsequent literature (Yeo et al., 2011). The default mode network (DMN), for example, a network which has been linked to idle-mind activities during the resting state, is less active in schizophrenia, especially in patients with certain disorganized symptoms (Gong et al., 2020; Lee et al., 2019b; Zhou et al., 2016). Similar impairments have been identified in the frontoparietal control network, and such impairments appear related to the degree of cognitive impairment experienced by the patient (Baker et al., 2014; Lewandowski et al., 2019). Such results lend further support to the disconnection hypothesis of schizophrenia (Friston et al., 2016), and encourages investigation into the mechanisms linking altered network connectivity and symptoms of psychosis.

Perhaps the most promising potential use of fMRI in schizophrenia is as a potential biomarker for early or complex diagnosis. Patients' outcomes are significantly improved if psychosis is identified and treated early, which makes diagnosis of prodromal and high-risk psychosis of critical importance (Correll et al., 2018; Aceituno et al., 2019). Neurophysiological evidence indicates that individuals with subclinical symptoms only rarely go on to develop a disorder, giving such symptoms a low diagnostic specificity and little predictive value (Addington et al., 2019; van Tricht et al., 2014). Additionally, the identification of patients in this stage of disease is complicated by the subjective nature of clinical diagnostic interviews, which can confound diagnosis in patients with multiple comorbid conditions (Compean and Hamner, 2019; Slotema et al., 2018). A major goal of research, therefore, is to identify an imaging biomarker – a feature of an fMRI scan which could reliably identify patients with schizophrenia separately from healthy controls. Such a biomarker would need to be both sensitive and specific, but would be able to objectively identify those with the disorder (Tognin et al., 2020). Developing imaging biomarkers is an active area of work, and a key step

in leveraging neuroimaging to improve outcomes in psychosis.

BACKGROUND

Signal Processing and Time-Frequency Analysis

In resting state fMRI analysis, the activation within a voxel over the course of multiple imaging volumes can be represented by a time series, and can thus be analyzed using the techniques of digital signal processing. Such techniques are mathematically defined for any data that can be represented as a time series, that is, a collection of discrete values associated with given points in time. These series are common within science and engineering, where they can represent signals as diverse as market performance and electroencephalography data. When the value of such signals are represented as functions of time, they are said to be "time-domain signals" (Alkin, 2014). One of the most important properties of such signals is the measure of the time between sample points, or its inverse, the number of data points every second. These quantities are referred to as the sampling time (T_s) or sampling rate (F_s) respectively. This definition of time-domain signals allows for the application of mathematical tools, such as convolution or autocorrelation, to any data that can be represented as a time series (Nielsen, 2019).

Different ways of organizing information can allow alternative frameworks for analysis. In physics, for example, while elementary problems use Newtonian mechanics (which use forces and motion to describe the motion of an object over time), Lagrangian dynamics (which describes dynamical behavior in terms of energy) can lead to simpler models for understanding the behavior of certain system's (Greenwood, 1987). Similarly, digital signals are commonly represented, instead of as a time series, in terms of the frequencies which sum to form them. Any function can be represented as the sum of an infinite series of sine waves of specific amplitude and frequency. The list of the amplitudes of these waves are known as the Fourier series. Digital signals,

that is to say, real data, are discretized, and have Fourier series given instead by the discrete Fourier transform (DFT) (Alkin, 2014). Rather than representing the data by a single amplitude at a series of points in time, data in the frequency domain (Figure 1) is represented by the amplitude and phase of the component sine wave at a series of discrete frequencies. As an example of a situation where this approach provides unique information, Figure 2 shows a representation of the contribution of a 60Hz signal (as if from a power line) on simulated EEG data. In the time domain, this signal simply seems to add noise and variability to the lower-frequency signals, but in the frequency domain, it is clearly represented as a peak at 60Hz (Luck, 2014; Cohen, 2014).

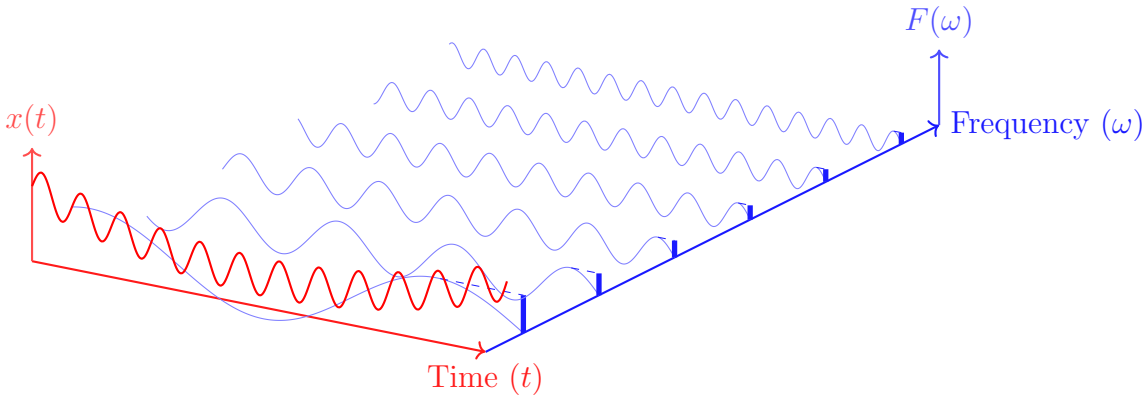

Figure 1: Time vs. Frequency Domain Signal Representation

The time-domain signal (red) can be represented by the amplitude of the sine waves which sum to form it.

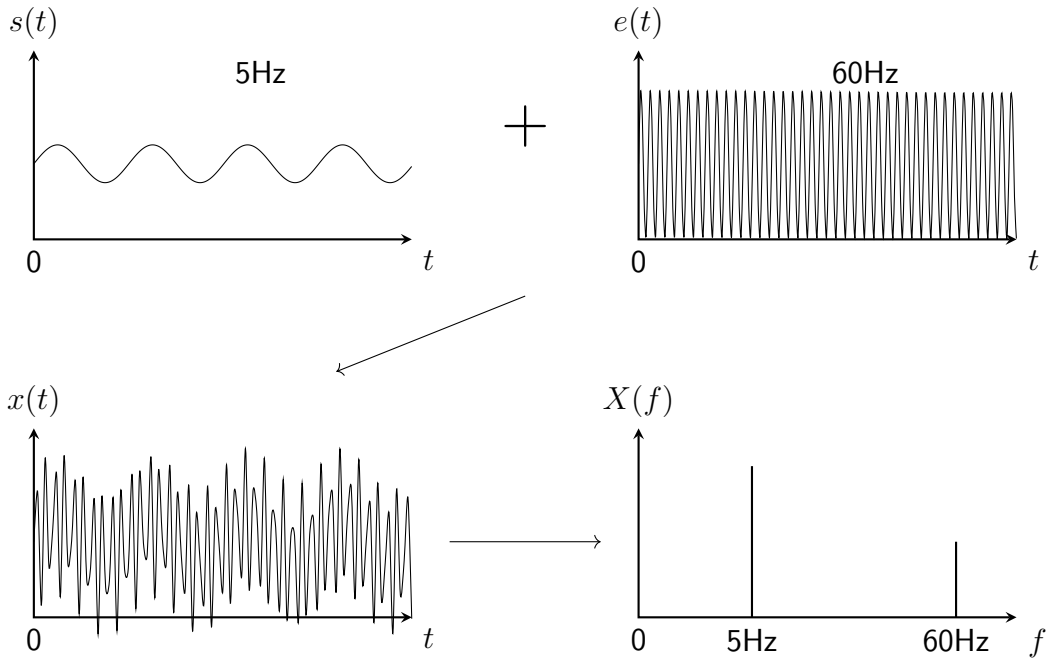

Figure 2: Powerline Contamination in the Frequency Domain

The summation of a 5Hz and 60Hz signal resembles noise in the time domain, but shows two distinct peaks in the frequency domain.

The Fourier transform only changes the form in which a signal's information is stored; it cannot generate new information about a signal. All of the information (the specific values contained in a signal, compared to all the values they could take) contained in a signal is obtained at the time of recording. The quantity of information can not increase, despite the transform (Cover and Thomas, 2006). For a time-domain signal, sampled at f_s for N points at a resolution of 1 byte per sample, the information is represented by N numbers representing the signal value x_n. When the DFT is applied to this signal, it is represented by values of X_n, with $n = 0, 1, 2...N$, with the corresponding frequencies of $f_n = f_s \frac{N-1}{N}$. As is evident in Figure 3, the second half of these values carry the same values as the first half, implying that the frequency-domain representation somehow contains half as much data as the time-

domain signal. X_n, however, is a complex value, where each data point contains two bytes of data: a real component and imaginary component. The result is that the frequency domain representation of a signal contains exactly as many bytes, and thus information as the time-domain representation, and in fact can be moved back into the time domain by inverting the transform. The information does not change, only the way it is represented. This is analogous to translating a sentence between two different languages. Because the amount of information is conserved, it is possible to know the value of every time point, or the value of every frequency point, but not the value of every frequency at every time point. This result is often described as a time-frequency uncertainty limit not unlike the Heisenberg uncertainty principle in quantum mechanics (Liu et al., 2018; Shinde and Gadre, 2001).

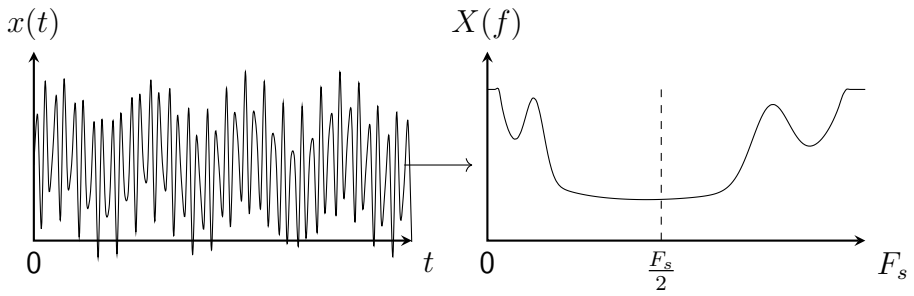

Figure 3: Fourier Transform (Real Component Only)

The Fourier transform translates data between the time and frequency domains without loss of information. The frequency domain signal is mirrored around f=0, and extends repeatedly in both directions.

When applied to neural time series, the Fourier transform can provide insight into physiological oscillatory patterns. In EEG research, for example, the Fourier transform is applied to a channel of electrode data representing the electrical potential at the scalp. Neurons transmit electrical pulses in a periodic way, and the signals recorded at these electrodes can be thought of as a summation of many different such

periodic neuronal signals (Nunez and Srinivasan, 2006). The Fourier transform shows the frequency of the neural sources during different brain states. Relaxed participants, for example, show increased activity between 8Hz and 12Hz, a phenomenon described as alpha waves (Liu et al., 2019; Allen et al., 2018). Unfortunately, because the Fourier transform represents the signals as a function of frequency rather than time, it cannot show how the strength of these waves varies over the course of an experiment. In other words, the Fourier transform assumes that a signal is stationary, meaning that its statistical properties do not vary with time. (Pierce, 1980; Nielsen, 2019).

Nonstationary data can be analyzed using the techniques of time-frequency analysis, a family of techniques which seeks to explore the way the frequency domain of a signal changes with time. The simplest method of doing so is by dividing the original signal and computing the Fourier transform for each of these segments – a process known as the short time Fourier transform (Figure 4). While this technique does allow for a crude comparison of the frequency spectrum at different points in time, the shorter length of the segments reduces the frequency resolution compared to the original transform. A more advanced form of this analysis, the sliding-window Fourier transform, can provide an arbitrary level of frequency precision but provides minimal information about the start and end of a signal (Richardson and Eddy, 2018). Both of these techniques have been applied to investigate the nonstationarities of neural time series (Zhou et al., 2019; Fu et al., 2018).

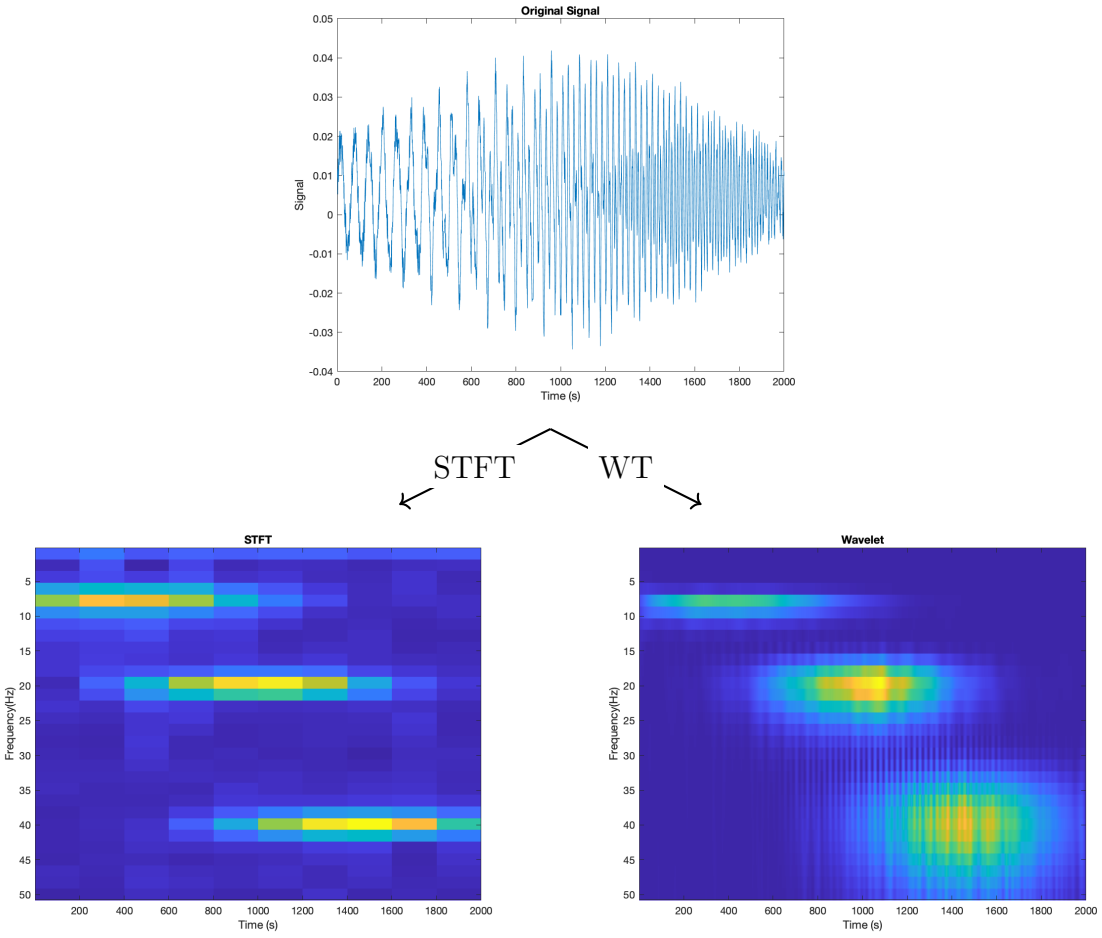

Figure 4: Short Time Fourier and Wavelet Transform Results

The result of the application of the STFT and WT to the same signal, generated by the summation of three temporally localized sine waves. All three of these components are visible in the result, but the transforms represent the information in different ways.

A more elegant technique for time-frequency analysis is a mathematical procedure called the wavelet transform (WT). In the Fourier transform, a sine wave at a specific frequency is compared to the time domain signal. Instead of using sine waves, the WT uses wavelets: oscillatory functions which only have values at certain times times (Cohen, 2019). A common example is the Morlet wavelet (Figure 5), which is a sine

wave multiplied by a gaussian to produce a temporally-localized sine wave. This pattern, called the kernel, is convolved with the time series signal to give a result which represents the strength of the wavelet's frequency at every point in time. When this is done with a collection of wavelets at different frequencies (a wavelet family), the result is a 2D data structure which represents the power in each frequency at every time point. Because the 2D data cannot contain more information than the original signal, there is uncertainty in this result. The nature of this uncertainty is controlled by the width of the wavelet's gaussian (the wavelet parameter c): a wider wavelet will be more precise in identifying power at the specific frequency, but less precise at localizing that activity in time. This uncertainty will be reflected in the appearance of "smearing" of a signal over the time and frequency domains (Grossmann and Morlet, 1984; Cohen, 2014).

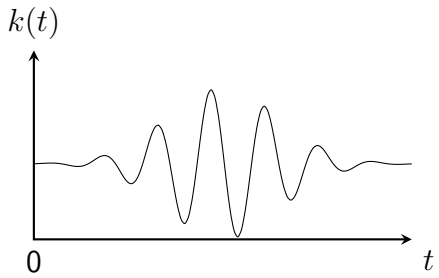

Figure 5: Morelet-style Wavelet Kernel

The kernel convolved against raw data in order to generate the morlet wavelet transform at the kernel's center frequency.

Resting State fMRI Analysis

By treating the images acquired during an fMRI scan as a time series, the techniques of signal processing can be used to generate unique insight into underlying neural funciton. If fMRI sequences are run while a participant is resting, rather than

when they are engaged in a specific task, the scan is termed a resting state fMRI (RS-fMRI) scan (Di et al., 2015; Amaro and Barker, 2006; Biswal et al., 1995). This technique gives researchers insight into the underlying dynamics of baseline neuronal activation which other designs seek to average out.

One common analysis technique in RS-fMRI is the identification and extraction of functional brain networks. Functional networks are areas of the brain which activate together, and have fMRI time series with strong interrelationships (Friston, 2011). There are a variety of techniques for detecting such covarying voxels. Simpler methods include bivariate correlation between voxels in different regions of interest, while more advanced techniques use independent component analysis to minimize the mutual information between spatially distinct clusters (Biswal et al., 1995; Calhoun et al., 2009). These clusters have been explored and defined as functional networks related to different neural systems (Yeo et al., 2011). The default mode network (DMN), for example, is a collection of cerebral areas which is active during the resting state, and is specifically tied to idle cognition (Lee et al., 2019a). The DMN is dysregulated in schizophrenia, showing altered within-network connectivity as well as differences in its relationship with other functional networks (Hu et al., 2017; Lee et al., 2019a; Öngür et al., 2010). The connections within these other networks, such as the frontoparietal control network (FPN) have also been shown to be impaired in Schizophrenia (Lewandowski et al., 2019).

An alternative technique for exploring the spatial patterns within an RS-fMRI dataset explores the way spatially contiguous voxels covary. In Regional Homogeneity (ReHo) analysis, the Kendall Coefficient of Concordance (KCC) is calculated between a voxel and its neighbors (Zang et al., 2004). The resulting image shows which areas of the brain exhibit greater levels of local synchronization, results which track physiological and other imaging measures (Yuan et al., 2013). Patients with

schizophrenia demonstrate altered levels of ReHo in certain functional areas, including those involved in sensory processing (Xu et al., 2015). In addition, levels of ReHo in thalamic areas are correlated with a patient's symptom burden prior to antipsychotic treatment (Zhao et al., 2019). In some voxels, these changes are related to the underlying frequency of BOLD fluctuations (Yu et al., 2013).

The transformation of fMRI time series into the frequency domain has also yielded interesting results. The Amplitude of Low Frequency Fluctuation (ALFF) metric is defined as the average of the Fourier transform (from 0.01Hz to 0.08Hz) of the BOLD signal within a voxel (Zang et al., 2007). A related metric, fractional ALFF, divides ALFF by the power in all frequencies, rather than just the lower frequency bands (Zou et al., 2008). Compared to healthy controls, patients with schizopphrenia show large areas of decreased ALFF in the occipital lobe (Hare et al., 2016). Additionally, patients with hallucinations show increased ALFF in the thalamus and parahippocampal gyri compared to patients without those symptoms, further demonstrating the role of sensory dysfunction in the disease (Alonso-Solís et al., 2017). In a 2020 meta-analysis, Gong et al. demonstrated consistently decreased ALFF in the postcentral gyri, precuneus, and right occiptal lobe and increased ALFF in areas of the putamen, frontal and temporal gyri, and anterior cingulate.

Techniques of time-frequency decomposition can be leveraged to perform novel analyses of fMRI datasets. One such application is to use the Wavelet transform in order to calculate ALFF, which increases the sensitivity and reproducibility of voxel-wise results (Luo et al., 2020). So far, wavelet-ALFF has been applied in mild cognitive impairment, but has not been applied to Schizophrenia (Cui et al., 2021). Another technique, termed dynamic ALFF (dALFF) applies a low-resolution sliding-window Fourier transform to the fMRI time series, producing maps of ALFF at multiple points during an RS-fMRI experiment (Tang et al., 2018). This technique has

been applied to generalized anxiety disorder, with striatal dALFF correlating with symptom burden (Cui et al., 2020). dALFF has also been combined with functional connectivity in Schizophrenia, in a study which demonstrated that the correlated, dynamic patterns of both ALFF and functional connectivity were modified in the disorder (Fu et al., 2018). Wavelet analysis has also been used in literature investigating dynamic functional connectivity, wherein it can generate frequency-specific profiles of neural connection (Yaesoubi et al., 2017b,a; Chang and Glover, 2010).

The Hilbert-Huang Transform

The intersection of signal processing and RS-fMRI is clearly a developing area of research. Understanding the natural patterns of activity present in the resting brain leads to insights regarding cerebral function and organization, can reveal the ways these dynamics are impacted in disease, and may lead to diagnostic and treatment biomarkers. The nonstationary time series of a voxel's BOLD activation is an especially exciting target for the application of time-frequency decomposition, which can reveal the dynamic nature of neural behavior. The leading techniques, such as the wavelet transform, are increasingly being applied, although the WT's limitations may hamper the understanding of complex dynamic behavior. One potential time-frequency decomposition method, the Hilbert-Huang transform, is of special interest. It minimizes the smearing evident in other techniques by only analyzing specific empirical components of the underlying data, and so is a potential tool for careful investigation of time-frequency dynamics.

The first operation of the Hilbert-Huang transform, called Empirical Mode Decomposition (EMD), breaks a time-domain signal into a number of Intrinsic Mode Functions (IMFs). An IMF is a simple oscillatory function which, like a sine wave,

is meant to represent the oscillatory components of a signal. Unlike a sine wave, however, it has a variable frequency, amplitude, and phase, and is defined purely by the data in the original time series, rather than an analytic function. An IMF must satisfy two conditions: the difference between the number of extrema and zero crossings must be equal to or less than one, and the two polynomials which connect the maxima and minima must have a mean value of zero (Huang et al., 1998). In order to construct an IMF from the original data, these two polynomials are constructed based on the maxima and minima of the time series, from which the mean of these polynomials is subtracted. This produces a candidate IMF, which is treated as the original data in another iteration of the process, a cycle demonstrated in Figure 6. When the candidate IMF h_k meets a stoppage criteria, it is called an IMF of the original data. If another IMF is to be extracted, the first is subtracted from the data, and this procedure – called sifting – is run again. Once a certain number of IMFs have been extracted (or another stopping criteria has been reached), any signal not captured by the IMFs is included in a residual term and reported, along with the IMFs, as the output of the process (Song et al., 2014). More mathematical detail about this process is given in the appendix.

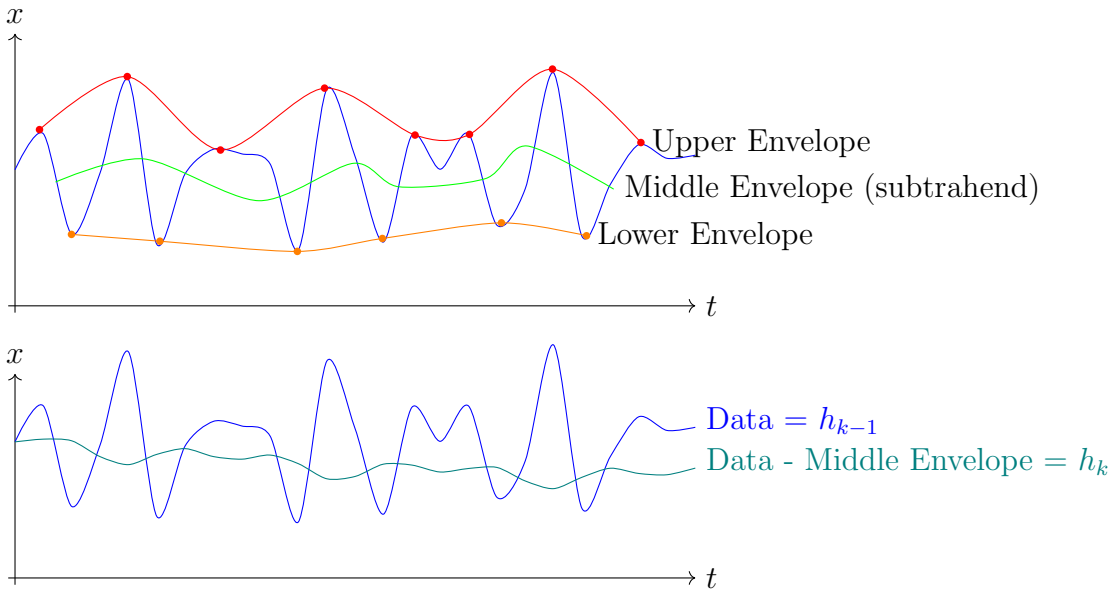

Figure 6: Emperical Mode Decomposition Sifting Process

The upper (red) and lower (orange) envelopes of the original data (blue) is averaged to produce the middle envelope (lime). This average is subtracted from the original data to perform sifting.

The EMD process takes place entirely in the time domain, and thus requires another step to be applicable in time-frequency analysis. This step is performed by the Hilbert transform, which takes a real signal and interpolates an imaginary component to produce a complex-valued signal. From this complex signal, the phase and frequency information can be calculated. Because no process can generate information that is not in the original signal, the imaginary component of the signal contains redundant information, but easily yields the parameters (amplitude, phase, and frequency) of a sine wave. When these are extracted from the Hilbert transform, they yield an estimate of the weighted average of oscillatory components of a signal at a given time. This averaging makes the Hilbert transform, when applied to raw data, difficult to interpret (Cohen, 2014). When working with neural time series, the

Hilbert transform is often combined with other ways of decomposing a signal, such as band-pass filtering (Yuan and Luo, 2012; Wang et al., 2015). By applying the Hilbert transform to the EMD of the signal, the IMFs are transformed into the frequency domain, giving the time-frequency characteristics of the empirical components of the signal. The resulting decomposition does not show the same smearing that is visible in the wavelet transforms, since it is not attempting to convey any information outside of the very specific IMFs (Liu et al., 2018).

When the Hilbert transform is applied to the EMD of a signal, the result is known as the Hilbert-Huang transform (HHT). The time-frequency plot of this result is shown in Figure 7, and can be further transformed into specific quantities which can be treated as discrete measurements of a given voxel's time series. One useful quantity is the energy of each IMF, which is given by the formula $E = \sum_{t=0}^{T} h^2(t)$. This produces a single imaging volume for each of the n IMFs, with each voxel taking on the value of the energy of that voxel's nth IMF. Each IMF can also yield a measure of average frequency, called the Hilbert weighted frequency (HWF). The HWF is the average of the frequency at every point in the time series, weighted by the square of the energy at that point (Xie and Wang, 2006). An alternative formulation of the HWF weights the frequency instead by the product of the frequency and amplitude (Oweis and Abdulhay, 2011). The HWFs of each IMF can also be averaged to produce an average frequency value for the entire voxel. These calculated image volumes of patients can be compared to those of controls (or correlated with behavioral variables) in order to investigate the relationship between the IMFs in various brain regions and phenotypic variables.

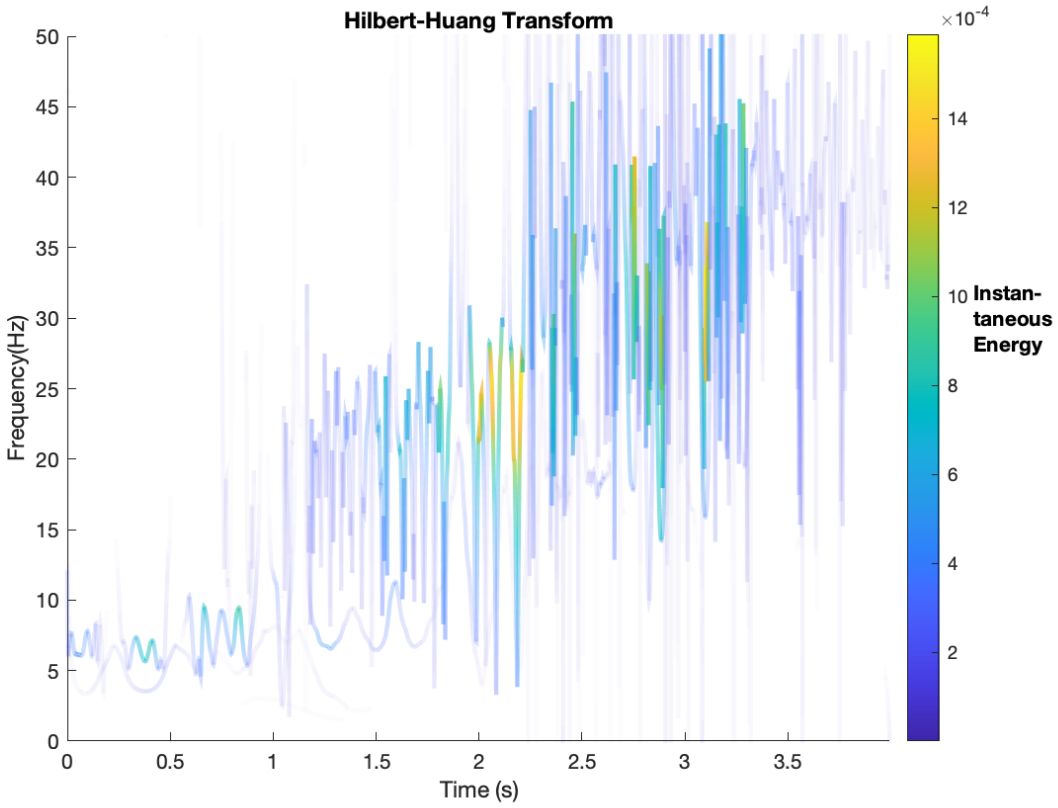

Figure 7: Hilbert-Huang Transform

An example of the Hilbert-Huang transform, applied to a time series of randomly generated data.

The HHT has only rarely been applied to fMRI data. In healthy subjects, the HHT has been used as an alternative basis to perform clustering and ReHo analysis. Using the IMFs instead of raw data, (Wu et al., 2017) performed a k-means clustering analysis to identify different loci of functional synchronization. IMFs have also been used as the time-series input to calculate the KCC during a ReHo analysis, a procedure which revealed drastic differences between ReHo measures in cortical and subcortical areas, with the former showing more complicated frequency-dependent behavior (Song et al., 2014). Looking at healthy subjects across the lifespan, Yang

et al. demonstrated that frequency modulation increased and amplitude modulation decreased (with modulation defined as the standard deviation of the quantity) as patients aged (Yang et al., 2018). In translational work, HWFs have been used as the input to a neural network which discriminated between the stages of mild cognitive impairment with 88% accuracy (Shi and Liu, 2020). HHT results can also differentiate healthy controls from patients with autism, who had higher HWFs in certain regions associated with the DMN (Zhang et al., 2021). The HWF measured around the limbic system was altered in patients with major depressive disorder in comparison to healthy controls, demonstrating promise for the technique in psychiatric disorders (Yu et al., 2018).

This study will apply the HHT to fMRI data in order to see if its unique ability to characterize nonstationary time series aides in the differentiation between patients with schizophrenia and healthy control subjects. Some differences in resting state measures, like ALFF, have already been reported and discussed, but they tend to present inconsistent results. If these inconsistencies are the result of the nonstationarities in the data, such analysis should provide results which are better able to differentiate patients and controls.

METHODS

fMRI Data Acquisition

Data were obtained from the Neuroimaging Tools & Resources Collaboratory (NITRC), specifically the Centers of Biomedical Research Excellence (COBRE) dataset. This contains the resting state scans of 72 patients with a DSM-IV diagnosis of Schizophrenia and 74 healthy controls free of DSM-IV diagnosis. Patients were scanned on a Siemens Tim Trio MR Scanner, with a field strength of 3T. Each participant had structural images (MPRAGE, TR = 2530ms, TE = 1.64, 3.5, 5.36, 7.22, 9.08ms, TI = 900ms, FA = 7°, Matrix 256x256x176mm, Voxel Size 1x1x1mm) collected for anatomical normalization in addition to a functional scan. The functional scan, collected during the resting state, was performed with a single-shot echo-planar imaging (EPI) sequence, with parameters TR = 2s, TE = 29ms, Matrix 64x64x32, and Voxel Size 3x3x4mm (Calhoun et al., 2012).

Image Preprocessing

Preprocessing of the 4D imaging volumes was performed in SPM12 (https://www.fil.ion.ucl.ac.uk/spm/) (Friston et al., 1994). The preprocessing pipeline included realigning the images to eliminate motion artifact and slice timing correction, both of which were conducted using the default parameters of SPM. The functional and structural images were then coregistered and normalized to $2mm^3$ voxels in the MNI152 stereotactic space. Finally, voxels were smoothed using an isotropic 8mm gaussian kernel. This process was repeated for all 146 subjects, and the results saved as normalized 4D imaging volumes.

Time Series Analysis

Preprocessed fMRI data was loaded into a custom MATLAB (The Mathworks, Inc., Natick, MA) workflow which incorporated utility functions from RESTplus v.1.24 (Jia et al., 2019). Voxels within the brain, as defined by a mask normalized to the common MNI152 space, were extracted and the time courses of signal within each of those voxels separately analyzed for their time-frequency parameters.

First, the wavelet transform was applied to each voxel time series. A family of Morlet wavelets with parameter $c = 2.5$ and center frequencies at 0.05Hz, 0.1Hz, and 0.15Hz, was convolved onto the time series, yielding time series representing activity in bands around those frequencies. Edge effects were eliminated by deleting all data less than a half-kernel width from the start and end of the series. The power and variance of the signal was calculated for each of these bands, and the values for these quantities assembled into an output image. The center frequencies for these wavelets were chosen in order to best approximate the standard range of frequencies which contribute to ALFF, with consideration given to avoiding information loss due to the long kernels required for low-frequency wavelets.

Similarly, Empirical Mode Decomposition was performed, using a sifting stop criterion of $SD = 0.2$, to extract a maximum of 5 IMFs from each time series. The energy of each of these IMFs was calculated according to $E_k = \sum_{t=0}^{T} {h_k}^2(t)$, where h_k is the kth IMF. The Hilbert transform was then applied to the IMFs, and the HWF was calculated as $HWF_k = \frac{\sum_{i=1}^{m} \omega_j(i) {a_j}^2(i)}{\sum_{i=1}^{m} {a_j}^2(i)}$, where w_j is the instantaneous frequency at every time point in the IMF and a_j is the amplitude. With an energy and HWF value for every voxel, the quantities were combined back into a 3D imaging volume. This process is illustrated in Figure 8.

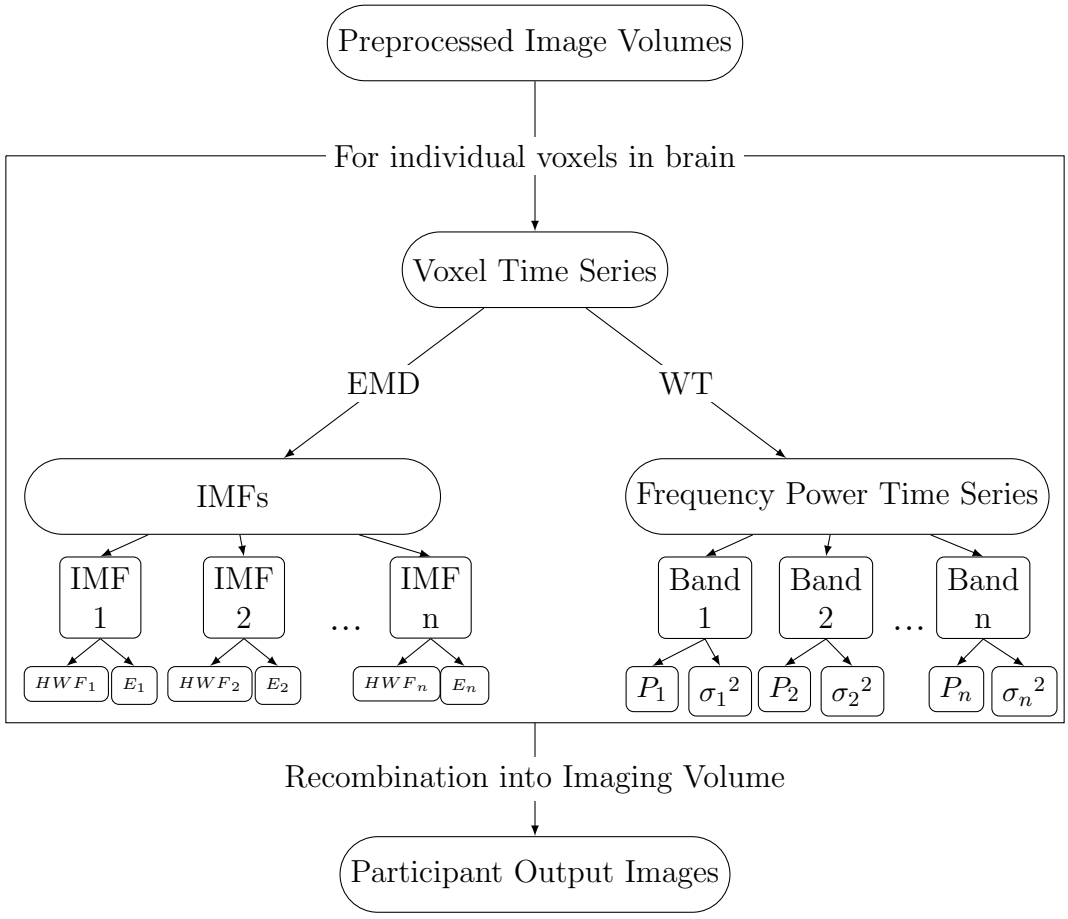

Figure 8: Pipeline Overrview

Illustration of all the transforms applied and measures generated during the present study. EMD produces several IMFs, from each of which is calculated energy and and HWF. The WT produces frequency power in the specified bands, which can yield average frequency power and variance. Each of these measures for every voxel are then recombined into a 3D imaging volume.

Group-Level Analysis

Statistical tests were conducted across every voxel of the standardized image space. For every voxel in the calculated images, an independent sample t-test was performed between the values of the patients' images and the values in the images of the control

participants. These t-maps were smoothed, in SPM, with an 8mm isotropic voxel. The significance of each value was tested using a cluster correction approach (in order to correct for multiple comparisons), with $\alpha = 0.001$ and the minimum cluster size of 200 voxels. This thresholding was performed in REST v.1.8 (Song et al., 2011). This process was applied to every image generated from the pipeline in Figure 8, and the results saved as an imaging volume with values of zero for nonsignificant comparisons and that of the t-statistic for significant voxels. This workflow is illustrated in Figure 9.

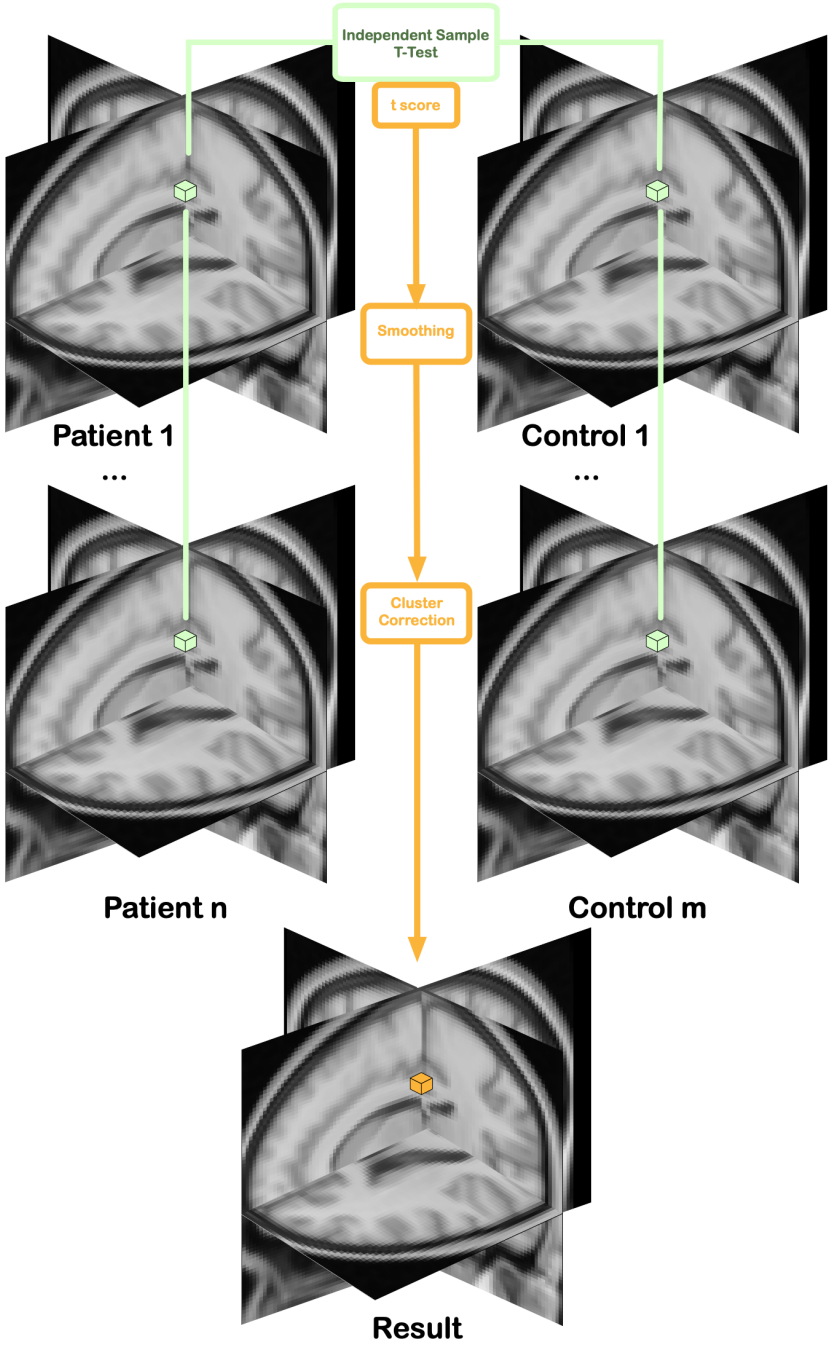

Figure 9: Statistical Analysis

Overview of process which generates the statistical maps of voxels with significant between-group differences. Every participant's value within the standardized imaging voxel is included in an independent sample t-test, which is then input to a simple cluster correction algorithm.

The ages within the schizophrenia group (M = 38.17 , SD = 13.89) and control group (M = 35.82 , SD = 11.58) were not significantly different (t(144) = -1.11, p = 0.27). Similarly, the gender distribution between the patients (80.6% male) and controls (68.9% male) was not significantly different (χ^2 (1, N = 146) = 2.61, p = 0.1). Therefore, no additional correction or regression was applied to the data.

RESULTS

Wavelet Tests

Six statistical tests were conducted corresponding to the power and variance within each of the three wavelet bands. The brain mask contained 292,019 voxels of 592,895 available in the 79x95x79 volume. Because the variance of each frequency band is a question being tested, the equal variances of the populations cannot be assumed, and so Satterthwaite's approximation is used to determine effective degrees of freedom. No voxels showed significant differences between patients and controls in band power within each of the three frequency bands tested (Figure 10).

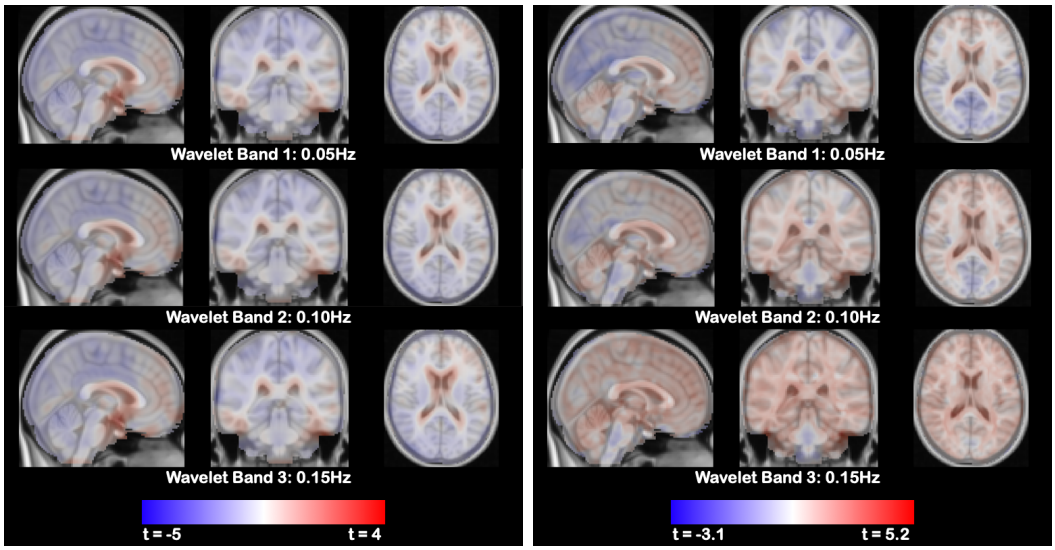

Figure 10: Power and Variance within Wavelet Bands

t values of comparison between patients and controls in statistical maps which have not been thresholded.

Similarly, no voxels showed significant differences in the variance within the first two frequency bands yielded by wavelet composition, although the parametric maps showed more qualitative variation between the three bands. The third wavelet band,

with a center frequency of 0.15Hz, did yield significant clusters of differences. These clusters were broadly centered around the ventricles, where the largest nonsignificant differences in the other maps are also observed. In all maps, other differences were largely diffuse throughout the volume. With the exception of differences in high-frequency variance within ventricles, the signal properties from the wavelet transform as applied yielded no significant differences between patients and controls.

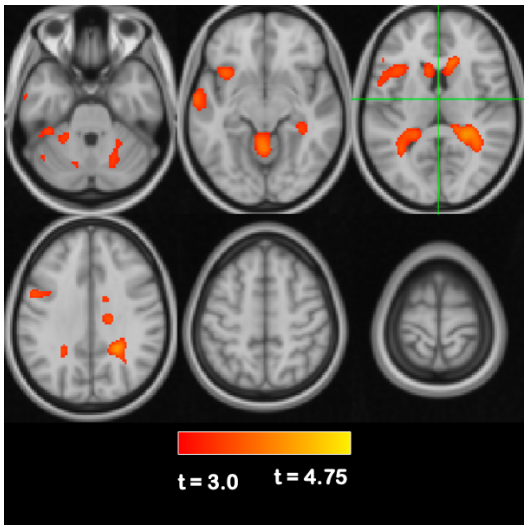

Figure 11: Cross Section of Voxel t-statistics for WT 3 Variance

Significant differences between patients and controls in the variance of the third wavelet band, after cluster correction.

IMF-wise Tests

The energy of each IMF was saved as a separate map, resulting in five voxel-wise t-tests between the participants and controls. Energy in IMFs 5, 4, 3, and 2 were not significantly different between patients and controls throughout the brain volume. IMF 1, however, showed significant differences between patients and controls in a variety of cerebral locations, as seen in Figure 12. Such differences were found primarily at the periphery of the brain, with the largest clusters in the frontal orbital

cortex, prefrontal gyrus, and supplementary motor cortex.

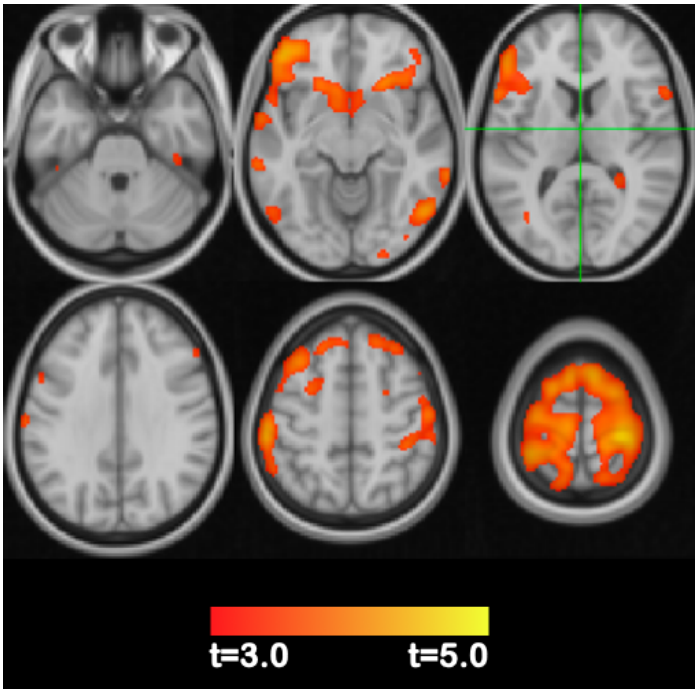

Figure 12: Cross Section of Voxel t-statistics for IMF 1 Energy

IMF1 had more energy in the schizophrenia group within peripheral areas, specifically the prefrontal gyrus, frontal orbital cortex, and supplementary motor cortex.

The other IMF-wise test conducted was the HWF of each IMF. IMFs one and two yielded clusters with significant differences in the HWF between patients and controls (Figure 13). The HWF of IMF 1 within the bilateral thalamus was significantly elevated in patients with schizophrenia compared to healthy controls, as was the HWF within the visual cortex. IMF 2 showed increased HWF for patients in clusters found in occipital areas. The remaining three IMFs showed no significant differences which survived cluster correction.

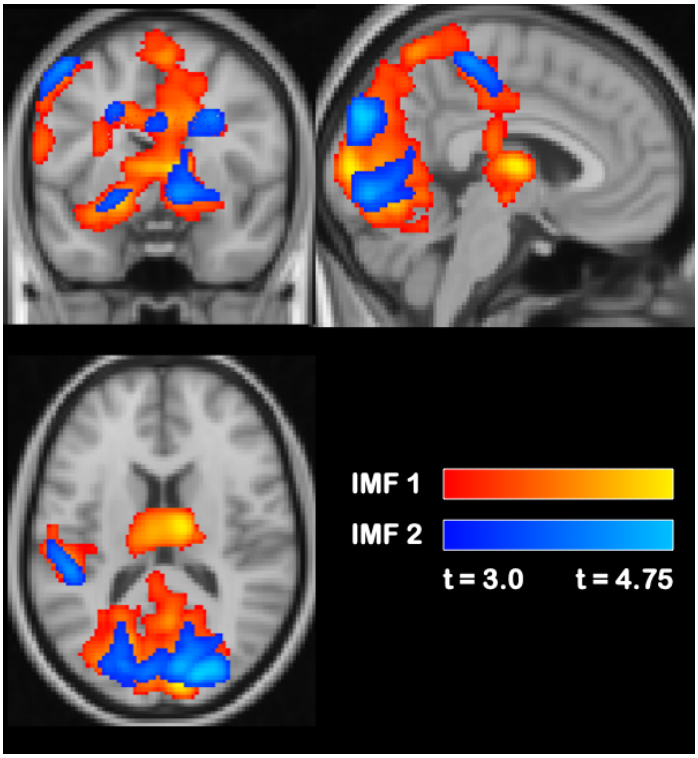

Figure 13: MIP of Voxel t-statistics for IMF HWFs

The first IMF showed increased HWF in patients within the thalamus and occipital cortex, while the second IMF showed increased HWF in patients only in occipital areas.

Voxel-wise Tests

The final test compared the average HWF across all of the IMFs. Patients with schizophrenia once again showed significantly increased frequencies compared to healthy controls across multiple areas of the brain (Figure 14). Like the IMF 1 energy map (Figure 12), many of the significant voxels are found around the outer boundaries of the brain, although considerably more voxels are found in the inner cerebrum than in the former case. Importantly, clusters can be found in both the thalamus as well as the postcentral gyrus, in both cases bilaterally.

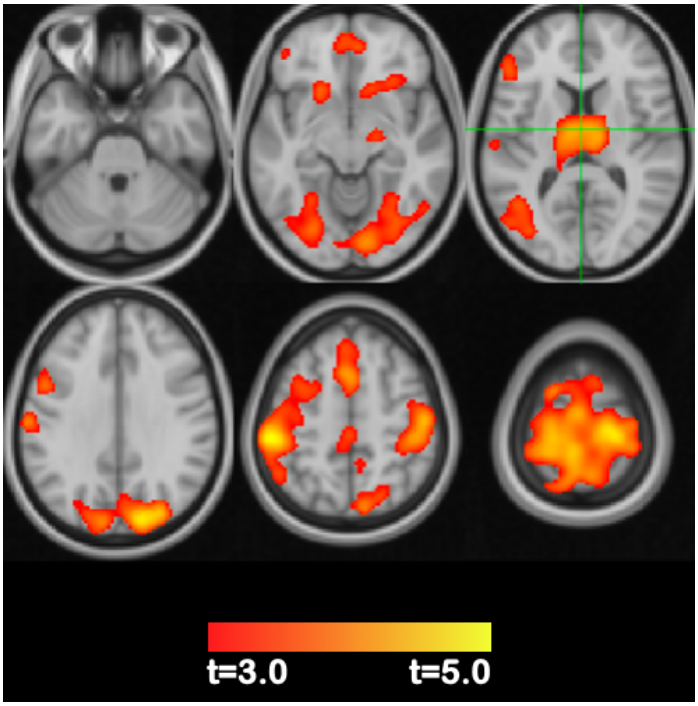

Figure 14: Cross Section of Voxel t-statistics for Mean HWF

The mean HWF across all IMFs was increased in patients for voxels within the thalamus and postcentral gyrus.

DISCUSSION

Wavelet Maps

Five out of the six measures derived from the wavelet transform failed to show any significant differences between patients and controls. In the statistical maps of the t-values, various brain areas showed elevated wavelet power while others showed decreased wavelet power in patients compared to controls. There were few qualitative differences between the spatial distribution of these values between the three frequency bands. There were more between-band differences in the maps of the variances of each band, however none of these differences were statistically significant. These results are broadly in line with the literature, which focuses only on the amplitude of fluctuations between 0.01Hz and 0.08Hz, and even then produces inconsistent results.

The remaining map, which did show significant differences, was of the variance of the signal within the third wavelet band, which was constructed with a center frequency of 0.15Hz. This is a relatively high frequency, and generally contains higher amounts of activity related to physiological noise (cardiac rhythms or respiration), rather than neural function (Josephs and Henson, 1999). This is reflected in the map of the results, which closely follow the anatomical features of the ventricles. This result therefore may represent physiological differences between patients and controls, but do not provide great insight into the neuronal dynamics underlying schizophrenia.

Hilbert-Huang Transform Results

The map of t-values comparing the energy of the first IMF (Figure 12) contains many significant clusters of voxels. These voxels are predominantly located on the

periphery of the brain, in areas close to the surface of the head. This is concerning because motion artifacts can be present at the periphery of the brain, exactly where these results are concentrated (Maknojia et al., 2019). Additionally, patients with schizophrenia are known to have differences in motor behavior, though the influence of this onto motion within fMRI scans has been disputed (Yoo et al., 2005). With that caution in mind, it is notable that large clusters of significant voxels are found in the prefrontal gyrus and motor cortex. Some of these clusters extend posteriorly into the rest of the parietal lobe, which is involved in sensory integration, a locus of disruption in schizophrenia.

The HWF of the first two IMFs showed significant differences between patients and controls. While similar concerns are warranted for these results as for the energy of the first IMF, there are significant differences in deeper brain structures. The cluster in the thalamus specifically is in alignment with results which show increased ALFF in thalamic areas (Alonso-Solís et al., 2017). Because the thalamus plays a critical role in the transmission and organization of sensory information, differences in its activation may reflect a neural basis for sensory abnormalities within schizophrenia. The HWF measure provides far more information about the properties of thalamic activation than ALFF, and a further exploration of the differences in thalamic HWFs may yield more precise understanding of the way function is disturbed in schizophrenia. The HWFs of IMF1 and IMF2 also show significant increases in the occipital lobe, specifically within areas associated with visual processing. These results are aligned with the findings of increased HWF in the thalamus, and frequency differences within sensory processing more broadly.

Similarly, the map of the average HWF across all IMFs show differences in areas associated with sensory processing. The thalamus, again, showed significant contrast between patients and controls. The same sensory and motor areas which were high-

lighted in the contrast of the first IMF's energy also showed large differences in the mean HWF image; these differences were not present in the contrasts of the individual IMF HWFs. A parsimonious explanation for this difference may be that individual HWFs are only slightly elevated in patients over controls, and the difference is only significant when all five elevated HWFs are considered together. The relationships between the mean HWF and IMF-wise HWF measures may contain diagnostic information, and are a target for further work.

Broadly, these results demonstrate the validity of applying the HHT to voxel time series in order to explore the pathophysiological differences observed in schizophrenia. Compared to measures produced from the WT, which displayed broad patterns but failed to reach significance, HHT-based measures showed significant differences in various areas. This analysis was exploratory and was designed to show the utility of these techniques, rather than to investigate the underlying dynamics of the frequency components extracted. Nevertheless, the increased HWFs and energies of the IMFs extracted from patients were concentrated in areas relating to sensory processing and motor behavior. Because sensory processing and motor activity is related to many symptoms of schizophrenia, more specific differences in these extracted components may yield a greater understanding of the underlying neuronal dynamics of the disorder.

Limitations and Expansion

This analysis has numerous limitations. To start, the COBRE dataset was collected more than ten years prior to this writing. With only 150 images per subject at a sampling rate of 0.5Hz, the lowest frequency which can be captured by wavelet convolution, while avoiding edge effects, is higher than the lower bands normally in-

cluded in ALFF. On the other end, such a sampling rate has a Nyquist frequency of 0.25Hz, and has difficulty detecting dynamics with more rapid oscillations. The advent of parallel multi-band imaging has improved the speed and quality of MRI scans in the time since these the COBRE images were collected, and so this analysis lacked modern imaging quality improvements (Blaimer et al., 2013). In addition, the nosology of and diagnostic techniques for psychosis have also advanced, most significantly with the arrival of the DSM-5 (and related SCID-5).

In response to these limitations, there are several possible directions in which to extend this work. In response to the relatively low quality of the data, a similar analysis could be applied to a more recent, optimized imaging sequence. The wavelet analysis, especially, was hampered by the limited number of resting state images in the time series. By acquiring more images with a higher sampling rate (such as the human connectome project's 1200 images with TR = 0.72s protocol), the time-varying dynamics of a wider variety of frequencies can be captured. Additionally, a more optimized scan protocol would contain sequences to map distortions in the $\vec{B}_0$ field so as to improve the spatial accuracy of the parametric maps, a goal which would also be aided by increasing the spatial resolution of the imaging matrix. The high likelihood of differences in patient motion between patients and controls also suggests that future work could leverage either improved head restraints or more advanced techniques for motion correction in order to minimize the confounding impact of motion.

The statistical techniques applied during this analysis were exploratory, and were designed to highlight areas which may contain differences in activation, rather than to test the contribution of specific volumes to these differences. With the identification of the thalamus and sensory areas as sites of differences in IMF behavior, future work could focus on testing predictions about the properties within specific regions

of interest (ROIs). By focusing on specific ROIs, such work could investigate more involved properties of the IMF signals. For example, there are multiple strategies for weighting the HWF which may take into account different features of the signal. These alternative weightings can include, for example, the product of frequency and amplitude, which would give more weight to higher frequencies (Oweis and Abdulhay, 2011). Modulation of the IMFs is an additional quantity which could be tested, as the disconnection hypothesis of schizophrenia would suggest differences in the variation in the activity of underlying neural sources. The phasic structure of each of the IMFs could also be a target of investigation. The phase locking value of two time series measures the similarity of the instantaneous phase of the signals. This calculation has been applied to different IMFs, and the interactions between the phases of different components may show significant differences (Zhang et al., 2014).

The measures generated from the HHT decomposition of the data could also be used as the basis for further explorations of functional connectivity states. Time-frequency decomposition has been used to identify different activation states of the brain's functional networks, but such analyses are generally restricted to either the short time Fourier or Wavelet transforms (Yaesoubi et al., 2015, 2017b; Fu et al., 2018). Using the instantaneous properties (phase, energy, frequency) of IMFs as a basis for identifying and categorizing different states of dynamic connectivity would be a natural extension of this work, as the IMFs may provide a more accurate representation of underlying activity. Another natural application of the HHT would be to decompose the time series of separate functional networks as extracted by ICA. By doing so, it may be possible to observe distinct nonstationary frequency components within these networks.

Broadly, the present study shows that the Hilbert-Huang transform has promise in the investigation of psychiatric imaging time-series. Images generated from mea-

sures based on the HHT showed clear statistical differences between patients with schizophrenia and healthy controls, and did so in patterns reflective of the symptoms of the disease. Further application of HHT-derived measures may yield yet more information, and may ultimately improve the understanding of and treatments available for psychotic disorders.

APPENDIX

This appendix contains a more rigorous, mathematical discussion of the Hilbert-Huang transform. It is being applied to a time series x which contains N time points, notated $x_n, n \in 1, 2, 3...N$. Because the time indexes will be important, the time at which each point is sampled is notated t_n

Empirical Mode Decomposition

The goal of empirical mode decomposition (EMD) is to extract the intrinsic mode functions (IMFs) from the underlying data. An IMF is a function which represents the non-stationary oscillatory modes imbedded in a time series. Mathematically, such functions must meet two criteria, for which additional notation must first be established.

For the time series x, the data points which correspond to local maxima are given by $a_j, j \in 1, 2, 3...N_a$, where N_a is the total number of maxima in x. The values of the maxima in x are therefore given by x_{a_j}. Similarly, the minima are given by $b_k, k \in 1, 2, 3...N_b$, and the values of those minima are x_{b_k}. The corresponding vectors for each of these elements are thus defined:

$$\begin{aligned} A &= [a_1, a_2, a_3, ...a_{N_a}] \\ X^A &= [x_{a_1}, x_{a_2}, x_{a_3}, ...x_{a_{N_a}}] \\ B &= [b_1, b_2, b_3, ...b_{N_b}] \\ X^B &= [x_{b_1}, x_{b_2}, x_{b_3}, ...x_{b_{N_b}}] \end{aligned}$$

These vectors of maxima and minima can be used to define polynomials, designed the upper and lower envelope of x. For every time point within x ($n \in 1, 2, 3...N$), the result of the cubic spline interpolation function is equivalent to this polynomial. While the precise formula for spline interpolation is outside the scope of this appendix,

the spline interpolation, and thus the upper envelope, of the series is given by ${s^a}_n = spline(A, X^A, n)$. The lower envelope is likewise ${s^b}_n = spline(N, X^B, n)$. This is written similarly to the MATLAB code which implements the spline function.

In practice, the spline function is combined with a padding function to ensure that there are sufficient data points to properly compute the spline at all points. This padding function adds a small number (e.g. 3) of data points to the beginning and ending of the vectors, with the position and values of those padding points given by sinusoidal extrapolation of the original function.

The first criteria in order for x to be considered an IMF is that the number of extrema and zero crossings must differ by no more than one. This is written as

$$N_a + N_b - N_z \leq 1$$

where N_z is the number of zero crossings. The second criterion is that the mean of the upper and lower envelopes must be zero at evert point, and can be written

$${s^b}_n = -{s^a}_n$$

for all $n \in 1, 2, 3...N$. With an IMF defined, the question then becomes how to determine the IMFs which comprise the signal x.

This is done through an iterative process called *sifting*, during which the mean of the envelopes is subtracted from the data (Figure 15).

$$c_{1n} = x_n - \frac{1}{2}({s^a}_n + {s^b}_n) \quad , \quad n \in 1, 2, 3...N$$

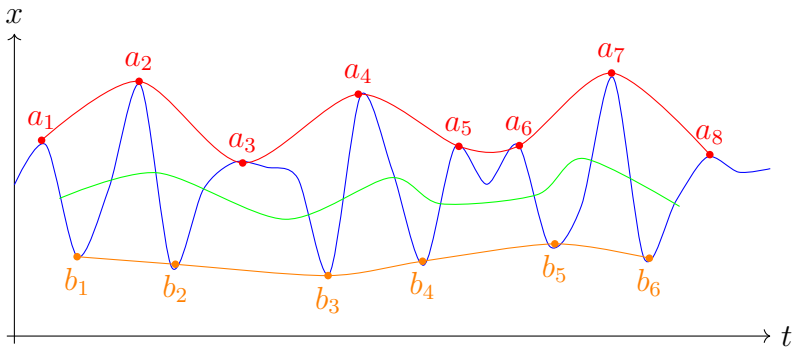

Figure 15: Sifting Process

The upper (red) and lower (orange) envelopes of the original data (blue) is averaged to produce the middle envelope (lime). This average is subtracted from the original data to perform sifting.

This subtraction produces the first candidate IMF, denoted c_1. c_1, however, still does not meet both criterion required of an IMF. In order to continue, the envelopes for c_1 are calculated (${s_{c_1}}^a{}_n$ and ${s_{c_1}}^b{}_n$), and the mean of these envelopes is subtracted from c_1 to yield a second candidate IMF, c_2.

$$c_{2n} = c_{1n} - \frac{1}{2}({s_{c_1}}^a{}_n + {s_{c_1}}^b{}_n) \quad , \quad n \in 1, 2, 3...N$$

Ideally, this proceeds until the resulting candidate IMF, c_k, satisfies both criteria for being an IMF. For computational efficency, however, sifting proceeds until an alternative criteria is met. This criteria represents the relative tolerance between successive iterations of the sifting process, and is given in Equation 1

$$SD_k = \sum_{t=0}^{T} \frac{|h_{k-1}(t) - h_k(t)|^2}{{h_{k-1}}^2(t)} \tag{1}$$

$$N_a + N_b \leq MaxExtrema \tag{2}$$

$$10log_{10}(\frac{x}{h}) \leq MaxEnergyRatio \tag{3}$$

When this quantity is below a certain value, typically set at 0.2, the candidate IMF c_n is said to be an IMF. The procedure is then restarted to find additional IMFs, using $x_n - c_{kn}$ as the initial data. This proceeds until a set number of IMFs are extracted from the signal, or until the stop criteria in equation 2 and equation 3) are met. The collection of extracted IMFs, along with the remaining initial data (the residual) are reported as the results of EMD.

Hilbert Transform

After the IMFs have been extracted through EMD, the second step of the Hilbert-Huang transform is to calculate the instantaneous frequency, energy, and phase of each IMF. This is done through manipulation of the result of the Hilbert transform (Eq. 4), which extends a real-valued signal into the complex domain.

$$H\{x_n\} = \frac{1}{\pi} \fint_{-\infty}^{\infty} \frac{x(\tau)}{t-\tau} d\tau \tag{4}$$

For a discrete signal, the discrete Hilbert transform is calculated by manipulation of the Fourier transform of that signal. The Fourier coefficients are rotated such that they correspond to the amplitudes of sin functions, rather than cosines: that is, they are phase shifted by 90°. The sum of the original coefficients and these rotated ones are converted back into the time domain, producing a complex-valued time domain signal from which signal parameters can be calculated.

Because the signal is now complex, it can be transformed from cartesian into polar coordinates, yielding, instead of a real and imaginary component, a phase and magnitude component for each point. These are the signals instantaneous magnitude and instantaneous phase. From these parameters, the instantaneous frequency – that is, the frequency of the signal at every point – is simply the derivative of the phase angle, scaled by the sampling frequency to produce a result in Hertz (Eq. 5).

$$f(t) = \omega(t) \cdot \frac{f_s}{2\pi} = \frac{d\theta}{dt} \cdot \frac{f_s}{2\pi} \tag{5}$$

REFERENCES

Aceituno, D., Vera, N., Prina, A. M., and McCrone, P. (2019). Cost-effectiveness of early intervention in psychosis: systematic review. *The British Journal of Psychiatry*, 215(01):388–394.

Addington, J., Stowkowy, J., Liu, L., Cadenhead, K. S., Cannon, T. D., Cornblatt, B. A., McGlashan, T. H., Perkins, D. O., Seidman, L. J., Tsuang, M. T., Walker, E. F., Bearden, C. E., Mathalon, D. H., Santesteban-Echarri, O., and Woods, S. W. (2019). Clinical and functional characteristics of youth at clinical high-risk for psychosis who do not transition to psychosis. *Psychological Medicine*, 49(10):1670–1677.

Alkin, O. (2014). *Signals and Systems*. CRC Press, 1st edition.

Allen, J. J. B., Keune, P. M., Schönenberg, M., and Nusslock, R. (2018). Frontal EEG alpha asymmetry and emotion: From neural underpinnings and methodological considerations to psychopathology and social cognition. *Psychophysiology*, 55(1):e13028.

Alonso-Solís, A., Vives-Gilabert, Y., Portella, M. J., Rabella, M., Grasa, E. M., Roldán, A., Keymer-Gausset, A., Molins, C., Núñez-Marín, F., Gómez-Ansón, B., Alvarez, E., and Corripio, I. (2017). Altered amplitude of low frequency fluctuations in schizophrenia patients with persistent auditory verbal hallucinations. *Schizophrenia Research*, 189:97–103.

Amaro, E. and Barker, G. J. (2006). Study design in fMRI: Basic principles. *Brain and Cognition*, 60(3):220–232.

American Psychiatric Association (2013). *Diagnostic and statistical manual of mental disorders*. American Psychiatric Association, Washington, DC, 5th edition.

Andreasen, N. C. and Carpenter, W. T. (1993). Diagnosis and Classification of Schizophrenia. *Schizophrenia Bulletin*, 19(2):199–214.

Arciniegas, D. B. (2015). Psychosis. *CONTINUUM: Lifelong Learning in Neurology*, 21:715–736.

Arias-Carrión, O., Stamelou, M., Murillo-Rodríguez, E., Menéndez-González, M., and Pöppel, E. (2010). Dopaminergic reward system: a short integrative review. *International Archives of Medicine*, 3(1):24.

Baker, J. T., Holmes, A. J., Masters, G. A., Yeo, B. T. T., Krienen, F., Buckner, R. L., and Öngür, D. (2014). Disruption of Cortical Association Networks in Schizophrenia and Psychotic Bipolar Disorder. *JAMA Psychiatry*, 71(2):109.

Biswal, B., Zerrin Yetkin, F., Haughton, V. M., and Hyde, J. S. (1995). Functional connectivity in the motor cortex of resting human brain using echo-planar mri. *Magnetic Resonance in Medicine*, 34(4):537–541.

Blaimer, M., Choli, M., Jakob, P. M., Griswold, M. A., and Breuer, F. A. (2013). Multiband phase-constrained parallel MRI. *Magnetic Resonance in Medicine*, 69(4):974–980.

Boyd, K. N. and Mailman, R. B. (2012). Dopamine Receptor Signaling and Current and Future Antipsychotic Drugs. In Gross, G. and Geyer, M. A., editors, *Current Antipsychotics*, volume 212, pages 53–86. Springer Berlin Heidelberg, Berlin, Heidelberg. Series Title: Handbook of Experimental Pharmacology.

Calhoun, V. D., Eichele, T., and Pearlson, G. (2009). Functional brain networks in schizophrenia: a review. *Frontiers in Human Neuroscience*, 3.

Calhoun, V. D., Sui, J., Kiehl, K., Turner, J., Allen, E., and Pearlson, G. (2012). Exploring the Psychosis Functional Connectome: Aberrant Intrinsic Networks in Schizophrenia and Bipolar Disorder. *Frontiers in Psychiatry*, 2.

Chang, C. and Glover, G. H. (2010). Time–frequency dynamics of resting-state brain connectivity measured with fMRI. *NeuroImage*, 50(1):81–98.

Clayson, P. E., Wynn, J. K., Infantolino, Z. P., Hajcak, G., Green, M. F., and Horan, W. P. (2019). Reward processing in certain versus uncertain contexts in schizophrenia: An event-related potential (ERP) study. *Journal of Abnormal Psychology*, 128(8):867–880.

Cohen, M. X. (2014). *Analyzing neural time series data: theory and practice*. MIT Press.

Cohen, M. X. (2019). A better way to define and describe morlet wavelets for time-frequency analysis. *NeuroImage*, 199:81–86.

Compean, E. and Hamner, M. (2019). Posttraumatic stress disorder with secondary psychotic features (PTSD-SP): Diagnostic and treatment challenges. *Progress in Neuro-Psychopharmacology and Biological Psychiatry*, 88:265–275.

Correll, C. U., Galling, B., Pawar, A., Krivko, A., Bonetto, C., Ruggeri, M., Craig, T. J., Nordentoft, M., Srihari, V. H., Guloksuz, S., Hui, C. L. M., Chen, E. Y. H., Valencia, M., Juarez, F., Robinson, D. G., Schooler, N. R., Brunette, M. F., Mueser, K. T., Rosenheck, R. A., Marcy, P., Addington, J., Estroff, S. E., Robinson, J., Penn, D., Severe, J. B., and Kane, J. M. (2018). Comparison of Early Intervention Services vs Treatment as Usual for Early-Phase Psychosis: A Systematic Review, Meta-analysis, and Meta-regression. *JAMA Psychiatry*, 75(6):555.

Cover, T. M. and Thomas, J. A. (2006). *Elements of Information Theory*. Wiley, 2nd edition.

Cui, L., Chen, K., Huang, L., Sun, J., Lv, Y., Jia, X., and Guo, Q. (2021). Changes in local brain function in mild cognitive impairment due to semantic dementia. *CNS Neuroscience & Therapeutics*, 27(5):587–602.

Cui, Q., Sheng, W., Chen, Y., Pang, Y., Lu, F., Tang, Q., Han, S., Shen, Q., Wang, Y., Xie, A., Huang, J., Li, D., Lei, T., He, Z., and Chen, H. (2020). Dynamic changes of amplitude of low-frequency fluctuations in patients with generalized anxiety disorder. *Human Brain Mapping*, 41(6):1667–1676.

Di, X., Fu, Z., Chan, S. C., Hung, Y. S., Biswal, B. B., and Zhang, Z. (2015). Task-related functional connectivity dynamics in a block-designed visual experiment. *Frontiers in Human Neuroscience*, 9.

Dong, M., Lu, L., Zhang, L., Zhang, Y.-S., Ng, C. H., Ungvari, G. S., Li, G., Meng, X., Wang, G., and Xiang, Y.-T. (2019). Quality of Life in Schizophrenia: A Meta-Analysis of Comparative Studies. *Psychiatric Quarterly*, 90(3):519–532.

Friston, K., Brown, H. R., Siemerkus, J., and Stephan, K. E. (2016). The dysconnection hypothesis (2016). *Schizophrenia Research*, 176(2-3):83–94.

Friston, K., Holmes, A., Poline, J.-B., Price, C., and Frith, C. (1996). Detecting Activations in PET and fMRI: Levels of Inference and Power. *NeuroImage*, 4(3):223–235.

Friston, K. J. (2011). Functional and Effective Connectivity: A Review. *Brain Connectivity*, 1(1):13–36.

Friston, K. J. and Frith, C. D. (1995). Schizophrenia: A disconnection syndrome? *Clinical Neuroscience*, 3(2):89–97.

Friston, K. J., Holmes, A. P., Worsley, K. J., Poline, J.-P., Frith, C. D., and Frackowiak, R. S. J. (1994). Statistical parametric maps in functional imaging: A general linear approach. *Human Brain Mapping*, 2(4):189–210.

Fu, Z., Tu, Y., Di, X., Du, Y., Pearlson, G., Turner, J., Biswal, B. B., Zhang, Z., and Calhoun, V. (2018). Characterizing dynamic amplitude of low-frequency fluctuation and its relationship with dynamic functional connectivity: An application to schizophrenia. *NeuroImage*, 180:619–631.

Gluck, M. A., Mercado, E., and Myers, C. E. (2016). *Learning and Memory*. Worth Publishers, 3rd edition.

Gong, J., Wang, J., Luo, X., Chen, G., Huang, H., Huang, R., Huang, L., and Wang, Y. (2020). Abnormalities of intrinsic regional brain activity in first-episode and chronic schizophrenia: a meta-analysis of resting-state functional MRI. *Journal of Psychiatry and Neuroscience*, 45(1):55–68.

Greenwood, D. (1987). *Principles of Dynamics*. Prentice Hall, 2nd edition.

Grossmann, A. and Morlet, J. (1984). Decomposition of hardy functions into square integrable wavelets of constant shape. *SIAM Journal on Mathematical Analysis*, 15:723–736.

Gur, R. E. and Gur, R. C. (2010). Functional magnetic resonance imaging in schizophrenia. *Translational Research*, 12(3):11.

Hakulinen, C., McGrath, J. J., Timmerman, A., Skipper, N., Mortensen, P. B., Pedersen, C. B., and Agerbo, E. (2019). The association between early-onset schizophrenia with employment, income, education, and cohabitation status: nationwide study with 35 years of follow-up. *Social Psychiatry and Psychiatric Epidemiology*, 54(11):1343–1351.

Hare, S. M., Ford, J. M., Ahmadi, A., Damaraju, E., Belger, A., Bustillo, J., Lee, H. J., Mathalon, D. H., Mueller, B. A., Preda, A., van Erp, T. G. M., Potkin, S. G., Calhoun, V. D., Turner, J. A., and Functional Imaging Biomedical Informatics Research Network (2016). Modality-Dependent Impact of Hallucinations on Low-Frequency Fluctuations in Schizophrenia. *Schizophrenia Bulletin*, page sbw093.

Hsiao, C.-Y., Lu, H.-L., and Tsai, Y.-F. (2020). Caregiver burden and health-related quality of life among primary family caregivers of individuals with schizophrenia: a cross-sectional study. *Quality of Life Research*, 29(10):2745–2757.

Hu, M.-L., Zong, X.-F., Mann, J. J., Zheng, J.-J., Liao, Y.-H., Li, Z.-C., He, Y., Chen, X.-G., and Tang, J.-S. (2017). A Review of the Functional and Anatomical Default Mode Network in Schizophrenia. *Neuroscience Bulletin*, 33(1):73–84.

Huang, N. E., Shen, Z., Long, S. R., Wu, M. C., Shih, H. H., Zheng, Q., Yen, N.-C., Tung, C. C., and Liu, H. H. (1998). The empirical mode decomposition and the Hilbert spectrum for nonlinear and non-stationary time series analysis. *Proceedings of the Royal Society of London. Series A: Mathematical, Physical and Engineering Sciences*, 454(1971):903–995.

Jauhar, S., Nour, M. M., Veronese, M., Rogdaki, M., Bonoldi, I., Azis, M., Turkheimer, F., McGuire, P., Young, A. H., and Howes, O. D. (2017). A Test of the Transdiagnostic Dopamine Hypothesis of Psychosis Using Positron Emission Tomographic Imaging in Bipolar Affective Disorder and Schizophrenia. *JAMA Psychiatry*, 74(12):1206.

Jia, X.-Z., Wang, J., Sun, H.-Y., Zhang, H., Liao, W., Wang, Z., Yan, C.-G., Song, X.-W., and Zang, Y.-F. (2019). RESTplus: an improved toolkit for resting-state functional magnetic resonance imaging data processing. *Science Bulletin*, 64(14):953–954.

Jin, H. and Mosweu, I. (2017). The Societal Cost of Schizophrenia: A Systematic Review. *PharmacoEconomics*, 35(1):25–42.

Josephs, O. and Henson, R. N. (1999). Event-related functional magnetic resonance imaging: modelling, inference and optimization. *Philosophical transactions of the royal society of london. series b: biological sciences*, 354(1387):1215–1228.

Kelleher, I. and Cannon, M. (2016). Putting Psychosis in Its Place. *American Journal of Psychiatry*, 173(10):951–952.

Kwapil, T. R., Gross, G. M., Silvia, P. J., Raulin, M. L., and Barrantes-Vidal, N. (2018). Development and psychometric properties of the Multidimensional Schizotypy Scale: A new measure for assessing positive, negative, and disorganized schizotypy. *Schizophrenia Research*, 193:209–217.

Lee, H., Lee, D.-K., Park, K., Kim, C.-E., and Ryu, S. (2019a). Default mode network connectivity is associated with long-term clinical outcome in patients with schizophrenia. *NeuroImage: Clinical*, 22:101805.

Lee, J., Jimenez, A. M., Horan, W. P., and Green, M. F. (2019b). fMRI biomarkers of social cognitive skills training in psychosis: Extrinsic and intrinsic functional connectivity. *PLOS ONE*, 14(5):e0214303.

Lewandowski, K. E., McCarthy, J. M., Öngür, D., Norris, L. A., Liu, G. Z., Juelich, R. J., and Baker, J. T. (2019). Functional connectivity in distinct cognitive subtypes in psychosis. *Schizophrenia Research*, 204:120–126.

Liu, Q., Ma, L., Fan, S.-Z., Abbod, M. F., Ai, Q., Chen, K., and Shieh, J.-S. (2018). Frontal EEG Temporal and Spectral Dynamics Similarity Analysis between Propofol and Desflurane Induced Anesthesia Using Hilbert-Huang Transform. *BioMed Research International*, 2018:1–16.

Liu, T., Zhang, J., Dong, X., Li, Z., Shi, X., Tong, Y., Yang, R., Wu, J., Wang, C., and Yan, T. (2019). Occipital Alpha Connectivity During Resting-State Electroencephalography in Patients With Ultra-High Risk for Psychosis and Schizophrenia. *Frontiers in Psychiatry*, 10:553.

Luck, S. J. (2014). *An Introduction to the Event-Related Potential Technique*. The MIT Press, 2nd edition.

Luo, F.-F., Wang, J.-B., Yuan, L.-X., Zhou, Z.-W., Xu, H., Ma, S.-H., Zang, Y.-F., and Zhang, M. (2020). Higher Sensitivity and Reproducibility of Wavelet-Based Amplitude of Resting-State fMRI. *Frontiers in Neuroscience*, 14:224.

Maknojia, S., Churchill, N. W., Schweizer, T. A., and Graham, S. J. (2019). Resting State fMRI: Going Through the Motions. *Frontiers in Neuroscience*, 13:825.

Menon, V. and Crottaz-Herbette, S. (2005). Combined EEG and fMRI Studies of Human Brain Function. *International Review of Neurobiology*, 66:291–321.

Nielsen, A. (2019). *Practical Time Series Analysis: Prediction with Statistics and Machine Learning*. O'Reilly Media.

Novak, K. D. and Foti, D. (2015). Teasing apart the anticipatory and consummatory processing of monetary incentives: An event-related potential study of reward dynamics: ERPs and reward dynamics. *Psychophysiology*, 52(11):1470–1482.

Nunez, P. L. and Srinivasan, R. (2006). *Electric Fields of the Brain: The Neurophysics of EEG*. Oxford University Press, 2nd edition.

Ogawa, S., Lee, T. M., Kay, A. R., and Tank, D. W. (1990). Brain magnetic resonance imaging with contrast dependent on blood oxygenation. *Proceedings of the National Academy of Sciences*, 87(24):9868–9872.

Öngür, D., Lundy, M., Greenhouse, I., Shinn, A. K., Menon, V., Cohen, B. M., and Renshaw, P. F. (2010). Default mode network abnormalities in bipolar disorder and schizophrenia. *Psychiatry Research: Neuroimaging*, 183(1):59–68.

Orellana, G. and Slachevsky, A. (2013). Executive Functioning in Schizophrenia. *Frontiers in Psychiatry*, 4.

Oweis, R. J. and Abdulhay, E. W. (2011). Seizure classification in EEG signals utilizing Hilbert-Huang transform. *BioMedical Engineering OnLine*, 10(1):15.

Parnas, J., Nordgaard, J., and S, V. (2010). The concept of psychosis: A clinical and theoretical analysis. *Clinical Neuropsychiatry*, 7:32–37.

Pierce, J. R. (1980). *An Introduction to Information Theory*. Dover Publications, 2nd edition.

Richardson, L. F. and Eddy, W. F. (2018). The Sliding Window Discrete Fourier Transform. *arXiv:1807.07797 [stat]*.

Saha, S., Chant, D., Welham, J., and McGrath, J. (2005). A Systematic Review of the Prevalence of Schizophrenia. *PLoS Medicine*, 2(5):e141.

Savica, R. and Benarroch, E. E. (2014). Dopamine receptor signaling in the forebrain: Recent insights and clinical implications. *Neurology*, 83(8):758–767.

Schmidt, A., Diwadkar, V. A., Smieskova, R., Harrisberger, F., Lang, U. E., McGuire, P., Fusar-Poli, P., and Borgwardt, S. (2015). Approaching a network connectivity-driven classification of the psychosis continuum: a selective review and suggestions for future research. *Frontiers in Human Neuroscience*, 8.

Shi, J. and Liu, B. (2020). Stage detection of mild cognitive impairment via fMRI using Hilbert Huang transform based classification framework. *Medical Physics*, 47(7):2902–2915.

Shinde, S. and Gadre, V. M. (2001). An uncertainty principle for real signals in the fractional fourier transform domain. *IEEE Transactions on Signal Processing*, 49(11):2545–2548.

Simeone, J. C., Ward, A. J., Rotella, P., Collins, J., and Windisch, R. (2015). An evaluation of variation in published estimates of schizophrenia prevalence from 1990-2013: a systematic literature review. *BMC Psychiatry*, 15(1):193.

Simon, G. E., Coleman, K. J., Yarborough, B. J. H., Operskalski, B., Stewart, C., Hunkeler, E. M., Lynch, F., Carrell, D., and Beck, A. (2017). First Presentation With Psychotic Symptoms in a Population-Based Sample. *Psychiatric Services*, 68(5):456–461.

Slotema, C. W., Blom, J. D., Niemantsverdriet, M. B. A., Deen, M., and Sommer, I. E. C. (2018). Comorbid Diagnosis of Psychotic Disorders in Borderline Personality Disorder: Prevalence and Influence on Outcome. *Frontiers in Psychiatry*, 9:84.

Song, X., Zhang, Y., and Liu, Y. (2014). Frequency Specificity of Regional Homogeneity in the Resting-State Human Brain. *PLoS ONE*, 9(1):e86818.

Song, X.-W., Dong, Z.-Y., Long, X.-Y., Li, S.-F., Zuo, X.-N., Zhu, C.-Z., He, Y., Yan, C.-G., and Zang, Y.-F. (2011). REST: A Toolkit for Resting-State Functional Magnetic Resonance Imaging Data Processing. *PLoS ONE*, 6(9):e25031.

Stepnicki, P., Kondej, M., and Kaczor, A. (2018). Current Concepts and Treatments of Schizophrenia. *Molecules*, 23(8):2087.

Tang, C., Wei, Y., Zhao, J., and Nie, J. (2018). The Dynamic Measurements of Regional Brain Activity for Resting-State fMRI: d-ALFF, d-fALFF and d-ReHo. In Frangi, A. F., Schnabel, J. A., Davatzikos, C., Alberola-López, C., and Fichtinger, G., editors, *Medical Image Computing and Computer Assisted Intervention – MICCAI 2018*, volume 11072, pages 190–197. Springer International Publishing, Cham. Series Title: Lecture Notes in Computer Science.

Tognin, S., van Hell, H. H., Merritt, K., Winter-van Rossum, I., Bossong, M. G., Kempton, M. J., Modinos, G., Fusar-Poli, P., Mechelli, A., Dazzan, P., Maat, A., de Haan, L., Crespo-Facorro, B., Glenthøj, B., Lawrie, S. M., McDonald, C., Gruber, O., van Amelsvoort, T., Arango, C., Kircher, T., Nelson, B., Galderisi, S., Bressan, R., Kwon, J. S., Weiser, M., Mizrahi, R., Sachs, G., Maatz, A., Kahn, R., McGuire, P., PSYSCAN Consortium, McGuire, P., Tognin, S., Fusar-Poli, P., Kempton, M., Modinos, G., Merritt, K., Mechelli, A., Dazzan, P., Gifford, G., Petros, N., Antoniades, M., De Micheli, A., Vieira, S., Spencer, T. J., Scarpazza, C., Hird, E., Kahn, R., Maat, A., van Hell, E., Winter, I., Cahn, W., Schnack, H., de Haan, L., Siegmann, D., Barkhof, J., Hendriks, L., de Wit, I., Crespo-Facorro, B., Tordesillas-Gutierrez, D., Setien-Suero, E., Ayesa-Arriola, R., Suarez-Pinilla, P., Ramirez-Bonilla, M., Garcia-de la foz, V. O., Glenthøj, B., Erlang Sørensen, M., Tangmose, K., Schæbel, H., Broberg, B., Rostrup, E., Lawrie, S., McDonald, C., Hallahan, B., Cannon, D., McLoughlin, J., Finnegan, M., Gruber, O., van Amelsvoort, T., Deckers, D., Marcelis, M., Vingerhoets, C., Arango, C., Díaz-Caneja, C. M., Ayora, M., Janssen, J., Rodríguez-Jiménez, R., Díaz-Marsá, M., Kircher, T., Falkenberg, I., Bitsch, F., Berger, P., Sommer, J., Raab, K., Jakobi, B., Nelson, B., McGorry, P., Amminger, P., McHugh, M., Galderisi, S., Mucci, A., Bucci, P., Piegari, G., Pietrafesa, D., Nicita, A., Patriarca, S., Bressan, R., Zugman, A., Gadelha, A., Rodrigues da Cunha, G., Soo Kwon, J., Kevin Cho, K. I. k., Young Lee, T., Kim, M., Bin Kwak, Y., Jeong Hwang, W., Weiser, M., Mizrahi, R., Kiang, M., Gerritsen, C., Maheandiran, M., Ahmed, S., Prce, I., Lepock, J., Sachs, G., Willeit, M., Lenczowski, M., Sauerzopf, U., Weidenauer, A., Furtner-Srajer, J., Kirschner, M., Maatz, A., Burrer, A., Stämpfli, P., Huber, N., Kaiser, S., Kawohl, W., Brammer, M., Young, J., Bullmore, E., and Morgan, S. (2020). Towards Precision Medicine in Psychosis: Benefits and Challenges of Multimodal Multicenter Studies—PSYSCAN: Translating Neuroimaging Findings From Research into Clinical Practice. *Schizophrenia Bulletin*, 46(2):432–441.

van Tricht, M. J., Ruhrmann, S., Arns, M., Müller, R., Bodatsch, M., Velthorst, E., Koelman, J. H., Bour, L. J., Zurek, K., Schultze-Lutter, F., Klosterkötter, J., Linszen, D. H., de Haan, L., Brockhaus-Dumke, A., and Nieman, D. H. (2014). Can quantitative EEG measures predict clinical outcome in subjects at Clinical High Risk for psychosis? A prospective multicenter study. *Schizophrenia Research*, 153(1-3):42–47.

Vrbova, K., Prasko, J., Ociskova, M., Kamaradova, D., Marackova, M., Holubova, M., Grambal, A., Slepecky, M., and Latalova, K. (2017). Quality of life, self-stigma, and hope in schizophrenia spectrum disorders: a cross-sectional study. *Neuropsychiatric Disease and Treatment*, 13:567–576.

Wang, Y., Liu, X., Zhang, Y., Zhu, Z., Liu, D., and Sun, J. (2015). Driving fatigue detection based on eeg signal. In *2015 Fifth International Conference on Instru-*

mentation and Measurement, Computer, Communication and Control (IMCCC), pages 715–718.

Wu, E. Q., Birnbaum, H. G., Shi, L., Ball, D. E., Kessler, R. C., Moulis, M., and Aggarwal, J. (2005). The economic burden of schizophrenia in the United States in 2002. *The Journal of Clinical Psychiatry*, 66(9):1122–1129.

Wu, X., Wu, T., Liu, C., Wen, X., and Yao, L. (2017). Frequency Clustering Analysis for Resting State Functional Magnetic Resonance Imaging Based on Hilbert-Huang Transform. *Frontiers in Human Neuroscience*, 11.

Xie, H. and Wang, Z. (2006). Mean frequency derived via Hilbert-Huang transform with application to fatigue EMG signal analysis. *Computer Methods and Programs in Biomedicine*, 82(2):114–120.

Xu, Y., Zhuo, C., Qin, W., Zhu, J., and Yu, C. (2015). Altered Spontaneous Brain Activity in Schizophrenia: A Meta-Analysis and a Large-Sample Study. *BioMed Research International*, 2015:1–11.

Yaesoubi, M., Allen, E. A., Miller, R. L., and Calhoun, V. D. (2015). Dynamic coherence analysis of resting fMRI data to jointly capture state-based phase, frequency, and time-domain information. *NeuroImage*, 120:133–142.

Yaesoubi, M., Miller, R. L., Bustillo, J., Lim, K. O., Vaidya, J., and Calhoun, V. D. (2017a). A joint time-frequency analysis of resting-state functional connectivity reveals novel patterns of connectivity shared between or unique to schizophrenia patients and healthy controls. *NeuroImage: Clinical*, 15:761–768.

Yaesoubi, M., Miller, R. L., and Calhoun, V. D. (2017b). Time-varying spectral power of resting-state fMRI networks reveal cross-frequency dependence in dynamic connectivity. *PLoS ONE*, 12(2):e0171647.

Yang, A. C., Tsai, S.-J., Lin, C.-P., Peng, C.-K., and Huang, N. E. (2018). Frequency and amplitude modulation of resting-state fMRI signals and their functional relevance in normal aging. *Neurobiology of Aging*, 70:59–69.

Yeo, B. T. T., Krienen, F. M., Sepulcre, J., Sabuncu, M. R., Lashkari, D., Hollinshead, M., Roffman, J. L., Smoller, J. W., Zöllei, L., Polimeni, J. R., Fischl, B., Liu, H., and Buckner, R. L. (2011). The organization of the human cerebral cortex estimated by intrinsic functional connectivity. *Journal of Neurophysiology*, 106(3):1125–1165.

Yerriah, J., Tomita, A., and Paruk, S. (2021). Surviving but not thriving: Burden of care and quality of life for caregivers of patients with schizophrenia spectrum disorders and comorbid substance use in South Africa. *Early Intervention in Psychiatry*, page eip.13141.

Yoo, S.-S., Choi, B.-G., Juh, R., Pae, C.-U., and Lee, C.-U. (2005). Head motion analysis during cognitive fMRI examination: Application in patients with schizophrenia. *Neuroscience Research*, 53(1):84–90.

Yu, H., Li, F., Wu, T., Li, R., Yao, L., Wang, C., and Wu, X. (2018). Functional brain abnormalities in major depressive disorder using the Hilbert-Huang transform. *Brain Imaging and Behavior*, 12(6):1556–1568.

Yu, R., Hsieh, M. H., Wang, H.-L. S., Liu, C.-M., Liu, C.-C., Hwang, T.-J., Chien, Y.-L., Hwu, H.-G., and Tseng, W.-Y. I. (2013). Frequency Dependent Alterations in Regional Homogeneity of Baseline Brain Activity in Schizophrenia. *PLoS ONE*, 8(3):e57516.

Yuan, F. and Luo, Z. (2012). The eeg de-noising research based on wavelet and hilbert transform method. In *2012 International Conference on Computer Science and Electronics Engineering*, volume 3, pages 361–365.

Yuan, R., Di, X., Kim, E. H., Barik, S., Rypma, B., and Biswal, B. B. (2013). Regional homogeneity of resting-state fMRI contributes to both neurovascular and task activation variations. *Magnetic Resonance Imaging*, 31(9):1492–1500.

Zang, Y., Jiang, T., Lu, Y., He, Y., and Tian, L. (2004). Regional homogeneity approach to fMRI data analysis. *NeuroImage*, 22(1):394–400.

Zang, Y.-F., He, Y., Zhu, C.-Z., Cao, Q.-J., Sui, M.-Q., Liang, M., Tian, L.-X., Jiang, T.-Z., and Wang, Y.-F. (2007). Altered baseline brain activity in children with ADHD revealed by resting-state functional MRI. *Brain & development*, 29(2):83–91. Place: Netherlands.

Zhang, H., Li, R., Wen, X., Li, Q., and Wu, X. (2021). Altered Time-Frequency Feature in Default Mode Network of Autism Based on Improved Hilbert-Huang Transform. *IEEE Journal of Biomedical and Health Informatics*, 25(2):485–492.

Zhang, J., Wang, N., Kuang, H., and Wang, R. (2014). An improved method to calculate phase locking value based on Hilbert–Huang transform and its application. *Neural Computing and Applications*, 24(1):125–132.

Zhao, X., Yao, J., Lv, Y., Zhang, X., Han, C., Chen, L., Ren, F., Jin, Z., Li, Y., and Sui, Y. (2019). Abnormalities of regional homogeneity and its correlation with clinical symptoms in Naïve patients with first-episode schizophrenia. *Brain Imaging and Behavior*, 13(2):503–513.

Zhou, L., Pu, W., Wang, J., Liu, H., Wu, G., Liu, C., Mwansisya, T. E., Tao, H., Chen, X., Huang, X., Lv, D., Xue, Z., Shan, B., and Liu, Z. (2016). Inefficient DMN Suppression in Schizophrenia Patients with Impaired Cognitive Function but not Patients with Preserved Cognitive Function. *Scientific Reports*, 6(1):21657.

Zhou, Q., Zhang, L., Feng, J., and Lo, C.-Y. Z. (2019). Tracking the Main States of Dynamic Functional Connectivity in Resting State. *Frontiers in Neuroscience*, 13:685.

Zou, Q.-H., Zhu, C.-Z., Yang, Y., Zuo, X.-N., Long, X.-Y., Cao, Q.-J., Wang, Y.-F., and Zang, Y.-F. (2008). An improved approach to detection of amplitude of low-frequency fluctuation (ALFF) for resting-state fMRI: Fractional ALFF. *Journal of Neuroscience Methods*, 172(1):137–141.

CURRICULUM VITAE